



LAWRENCE
LIVERMORE
NATIONAL
LABORATORY

Application of Ensemble Sensitivity Analysis to Observation Targeting for Short-term Wind Speed Forecasting in the Washington-Oregon Region

J. Zack, E. Natenberg, S. Young, G. V. Knowe, K. Waight, J. Manobianco, C. Kamath

October 5, 2010

Disclaimer

This document was prepared as an account of work sponsored by an agency of the United States government. Neither the United States government nor Lawrence Livermore National Security, LLC, nor any of their employees makes any warranty, expressed or implied, or assumes any legal liability or responsibility for the accuracy, completeness, or usefulness of any information, apparatus, product, or process disclosed, or represents that its use would not infringe privately owned rights. Reference herein to any specific commercial product, process, or service by trade name, trademark, manufacturer, or otherwise does not necessarily constitute or imply its endorsement, recommendation, or favoring by the United States government or Lawrence Livermore National Security, LLC. The views and opinions of authors expressed herein do not necessarily state or reflect those of the United States government or Lawrence Livermore National Security, LLC, and shall not be used for advertising or product endorsement purposes.

This work performed under the auspices of the U.S. Department of Energy by Lawrence Livermore National Laboratory under Contract DE-AC52-07NA27344.

Application of Ensemble Sensitivity Analysis to Observation Targeting for Short-term Wind Speed Forecasting in the Washington - Oregon Region

John Zack, Eddie Natenberg, Steve Young, Glenn Van Knowe,
Ken Waight, John Manobianco
AWS Truewind, LLC

Chandrika Kamath
Lawrence Livermore National Laboratory

October 1, 2010

1. Introduction

To economically and reliably balance electrical load and generation, electrical grid operators, also called Balancing Authorities (BA), need highly accurate electrical power generation forecasts in time frames ranging from a few minutes to six hours ahead. As wind power generation increases, there is a requirement to improve the accuracy of 0- to 6-hour ahead wind power forecasts. Forecasts covering this short look-ahead period have depended heavily on short-term trends obtained from the actual power production and meteorological data of a wind generation facility. Additional data are often available from Numerical Weather Prediction (NWP) models and sometimes from off-site meteorological towers near wind generation facilities.

The typical hub height of a wind turbine is approximately 80-m above ground level (AGL). So it would seem that building meteorological towers in the region upwind of a wind generation facility would provide necessary data to refine short-term forecasts for the 80-m AGL wind and power forecasts. However, this additional meteorological information typically does not significantly improve the accuracy of the 0- to 6-hour ahead wind power forecasts because processes controlling wind variability change from day to day and, at times, from hour to hour. Consequently, a meteorological tower location that provides beneficial forecast data at one time may not be useful a few hours later. It is also important to note that some processes causing significant changes in wind power production function principally in the vertical direction. These processes will not be detected by meteorological towers at off-site locations. For these reasons, it is quite challenging to determine the best type of sensors and deployment locations.

Methods have been developed recently that can be used to address the measurement deployment problem. These approaches rely on the use of NWP models to assess forecast sensitivity at a target location and look-ahead time to measurements made at model initialization time and points surrounding the region of interest. The techniques are based on the fundamental hypothesis that locations and variables with high sensitivity are good candidates for measurements, since information at those locations is likely to have the most impact on the forecast for the desired parameter, target area, and look-ahead period. Therefore, the methods have the potential to help determine the locations and parameters to measure in order to get maximum positive impact on forecast performance for a particular site.

To address the measurement deployment problem, Zack et al. (2010) applied the method known as Ensemble Sensitivity Analysis (ESA; Ancell and Hakim 2007; Torn and Hakim 2008). The ESA approach was initially designed to produce spatial fields of forecast sensitivity for a set of prior state variables selected by the user. No strategy for determining the optimal combination of multiple variable-location combinations had been developed in the previously published studies. Zack et al. (2010) developed the Multiple Observation Optimization Algorithm (MOOA) in order to determine the relative predictive value and optimal combination of different variables/locations from correlated sensitivity patterns.

In Zack et al. (2010), the ESA-MOOA approach was applied and evaluated for the wind plants in the Tehachapi Pass region for a period during the warm season. This research demonstrated that forecast sensitivity derived from the dataset was characterized by well-defined, localized patterns

for a number of state variables such as the 80-m wind and the 25-m to 1-km temperature difference prior to the forecast time. The sensitivity patterns produced as part of the Tehachapi Pass study were coherent and consistent with the basic physical processes that drive wind patterns in the Tehachapi area.

In this project, the ESA-MOAA approach is extended and applied to the warm season for the wind plant target areas of Klondike, Stateline and Hopkins Ridge located in the Washington-Oregon area of the northwest U.S. as shown in Figure 1. The objectives of this study were to identify measurement locations and variables that have the greatest positive impact on the accuracy of wind forecasts in the 0- to 6-hour look-ahead periods for the Mid-Columbia Basin wind generation area during the warm season and to establish a higher level of confidence in the ESA-MOAA approach for mesoscale applications.

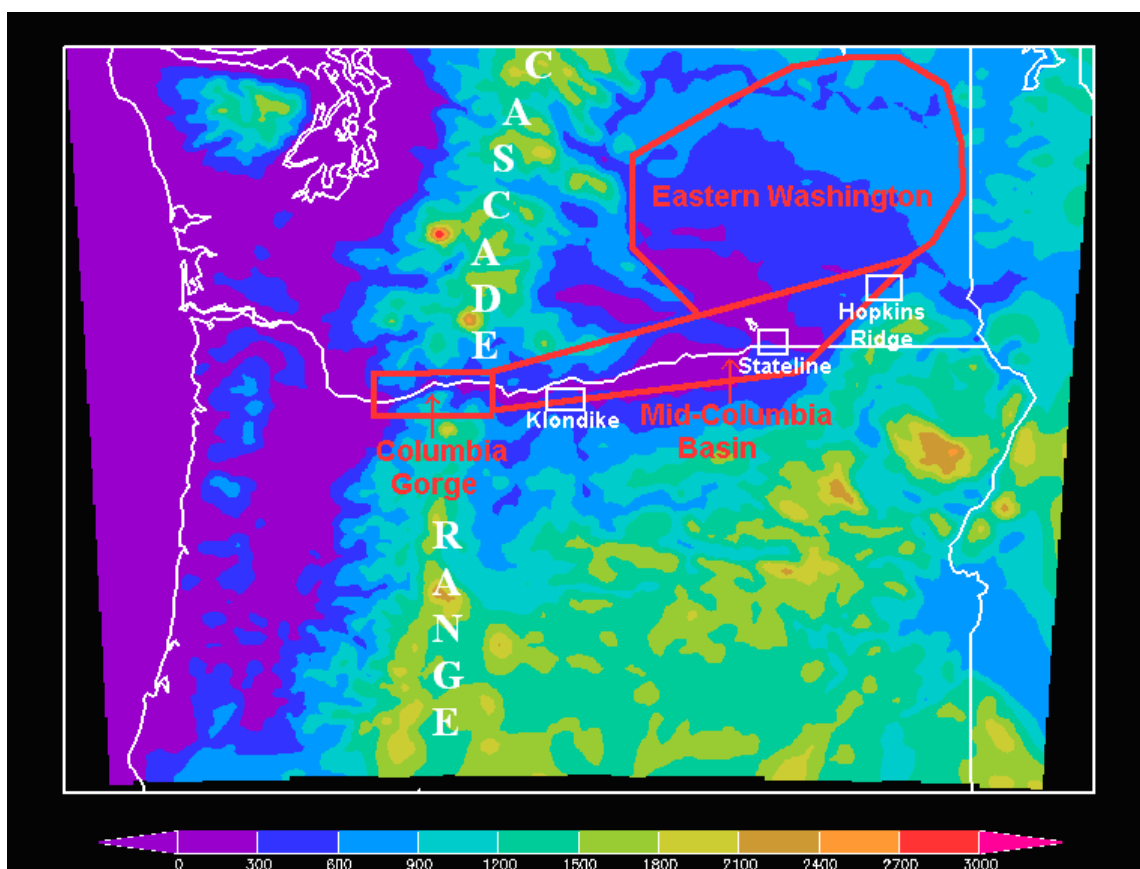


Figure 1. Geographical area used in the ensemble sensitivity analysis experiments. A matrix of 172 by 160 horizontal points with a spacing of approximately 4 km between points for 40 levels of the atmosphere at predetermined pressure levels (Appendix C) was overlaid on the Washington-Oregon domain for the experiment. The color shading depicts the terrain elevation (m) on the scale of the model grid. The white boxes denote the forecast target areas at Klondike, Stateline, and Hopkins Ridge with the broader geographic regions of the Columbia Gorge, Mid-

Columbia Basin and Eastern Washington highlighted in red outlines. The location of the Cascade Range is also indicated on the map.

The report is organized as follows. Section 2 highlights the methodology, Section 3 presents single-variable results, Section 4 covers multiple variable results, and Section 5 concludes with a summary and brief discussion of future work.

2. Methods

2.1 Description of ESA and EnKF

The ESA approach uses data generated by a set (ensemble) of perturbed NWP simulations for a sample time period to diagnose the sensitivity of a specified forecast variable (metric) for a target location to parameters at other locations and prior times [the initial condition (IC) state variable]. The ensemble of NWP simulations are produced by starting with a single initial state at the beginning of the analysis period and introducing statistical perturbations into the initial and lateral boundary conditions. For subsequent simulations after the first 6 hour forecast is produced, the initial state is a combination of the predicted and observed state. This process generates a set of simulations that differ from each other due to the perturbations. The number of simulations must be large enough to produce a statistically significant sample for the sensitivity calculations. Past studies have used 48 or more ensemble members for large-scale ESA applications (Torn and Hakim 2008).

The evaluation of simulation "spread" or differences between individual members of the ensemble was accomplished using an ensemble Kalman filter (EnKF; Houtekamer and Mitchell 1998; Evensen 2007). The EnKF attempts to balance the predicted and observed state of the atmosphere by estimating the likelihood of each state at any given time over the entire set of simulations in the ensemble. The EnKF assumes that model errors follow a normal (Gaussian) distribution in order to determine the most probable state of the atmosphere. The error is assessed using the time dependent spread and deviations obtained from the ensemble state with that of the observed state. Ensemble members are allowed to integrate forward in time while the filter monitors the spread in the ensemble. The EnKF assesses predictabilities (likelihood of occurrence) of the variable of interest for the target area by monitoring the change in the spread of the NWP ensemble.

In the ESA methodology, each initial state is used as the starting point for an NWP simulation. The NWP simulations are marched forward in time with periodic assimilation of observational data for some time referred to as the "analysis period". The periodic assimilation of measurement data serves to keep the model state from drifting too far from the actual atmospheric conditions. However, it is important to keep the spread of the ensemble within an acceptable range in order to obtain meaningful results.

Ensemble spread can be controlled by specifying characteristics of the IC perturbations through user-definable parameters. The initial perturbations are typically chosen to be relatively large

(i.e. larger than the observation uncertainty in the initial state) so that each ensemble member is unique. The ensemble spread then typically decreases during the "spin-up" of the ensemble and eventually comes into a balance within some general range that is indicative of the characteristics of the flow regime. For the Mid-Columbia Basin experiment, the range or standard deviation of horizontal wind speed was on the order of 3 to 7 m/s.

Excessive ensemble divergence is usually not a problem, since an increase in spread causes the members to adjust more to fit the available observed values. So initially large ensemble spread will eventually decrease by assimilating observations. On the other hand, convergence of ensemble members is more of an issue. A technique called covariance inflation (Anderson and Anderson 1999; Anderson 2007) is used to avoid ensemble convergence (i.e. large decrease in spread for highly predictable flows). Covariance inflation perturbs the members in areas of low spread based on user-specified values for the inflation parameters.

2.2 Model Configuration

The simulations were generated on a three-dimensional nested grid matrix of 120 x 120 horizontal points and 12-km spacing on the outer grid, and 172 x 160 points with 4-km spacing on the inner grid that covered most of Washington and Oregon. The inner grid area is depicted in Figure 1 and both grids are shown in Figure C1 (Appendix C). Both grids had 40 vertical layers at predefined pressure levels. The vertical grid spacing increases with height so there is higher resolution near the surface of the earth (see Appendix C for a listing of model levels).

A nested or multiple grid approach was used for this study to help simulate the flow in the Pacific Northwest region. The typical summer weather pattern in this region is dominated by large-scale atmospheric waves propagating from the Pacific Ocean eastward. A nesting strategy provides a lower resolution outer grid to capture these large scale flows upstream of the area of interest, while allowing boundary perturbations to grow and decay within the outer grid. It is important to keep the boundaries of the outer grid far enough removed from the inner grid to prevent interactions that would lead to ensemble instability. The inner nested grid is then used to resolve the terrain-induced circulations near the target region with a higher degree of detail.

The simulations were produced using version 2.2 of the Weather Research and Forecast (WRF) atmospheric model (Skamarock et al. 2005), and observational data were assimilated every 6 hours using an ensemble Kalman filter data assimilation procedure within the Data Assimilation Research Testbed (DART) software (Anderson 2001; Anderson et al. 2009). Data from the North American Mesoscale (NAM) model were used for initial and lateral boundary conditions. A total of 48 ensemble members were used in the analysis. Appendix A contains details of the WRF model configuration, ensemble Kalman filter data assimilation system, and the types of data assimilated.

The simulation period extended from 0000 UTC 1 May to 1800 UTC 19 June 2007. The first two days were designated as a "spin-up" period and the data were not used in the sensitivity calculations. Therefore, the analysis period covered 47 days from 3 May to 19 June 2007. The months of May and June 2007 were selected to encompass the period used for a ramp forecasting project sponsored by Bonneville Power Administration. Since a significant amount of analysis

has already been performed on the events during that period, results can be leveraged for the ESA experiments in this project.

Even with the use of a nested grid, the ensemble mean state became unstable during several simulations near eastern and southern lateral boundaries. In attempt to remove these instabilities the model was restarted with new perturbed IC and boundary conditions usually 2-3 days before the instability developed, with enough time to allow for ensemble spin-up.

These instabilities were related to covariance inflation of the ensemble which added strong perturbations to the assimilated model state and eventually grew into unphysical vertical flows along the lateral boundaries. In future studies, the nested grid should be extended to remove any correlations between assimilated observations and covariance inflation.

The simulation period was for six hours with data assimilation performed at the beginning of each period. A 6-hour data assimilation cycle was chosen to allow the model enough time to adjust to observational data. The sensitivities were calculated for two separate time periods from 0 to 3 hours and from 3 to 6 hours. The 1-hour sensitivities were computed from the initial time to hour 1 and from hour 3 to hour 4 of each simulation. The 1- and 3-hour sensitivities were computed because this is the look-ahead period of greatest interest to the grid operators. The second set of 1- and 3-h sensitivities were computed for each forecast in order to provide additional independent time periods for evaluation.

2.3 Description of IC Variables

The forecast metric (F) was defined as the average 80-m wind speed over the three target areas shown in Figure 1 (white boxes). The sensitivity calculation is not restricted to the same variable that is used to define the forecast metric. Sensitivity values can be calculated with respect to any quantity that can be derived from the basic set of prognostic variables in the NWP model used to generate the ensemble of simulations. The twelve IC state variables listed in Table 1 were evaluated.

Table 1. Twelve IC state variables used in the evaluation of sensitivity.

Wind Speed Related
80-m wind speed above ground level (AGL)
250-m wind speed AGL
1.5-km wind speed above mean sea level (AMSL)
3-km wind speed AMSL
Wind Shear Related
10-m to 80-m wind shear AGL
80-m to 500-m wind shear AGL
500-m to 1-km wind shear AGL
Temperature Related
2-m temperature AGL
2-m to 80-m temperature difference AGL
80-m to 1-km temperature difference AGL
80-m to 500-m temperature difference AGL
500-m to 1-km temperature difference AGL

The twelve IC parameters can be grouped into three categories: (1) Single level sensitivities, which include wind speed at various levels and 2-m temperature, (2) vertical wind shear, and (3) vertical temperature gradient. The wind shear and temperature gradients were computed for various layers from near the surface to a level of 1-km AGL.

Winds at turbine hub height (80 m) are typically quite useful for predicting the same quantity within the target location at later times. In order to get a sense of the variation in sensitivity to wind speed with height, three other levels at 250-m AGL, 1.5-km AMSL, and 3-km AMSL were also examined. The near-surface temperature, wind shear and vertical temperature difference variables were chosen because they are useful for defining the characteristics of the surges of marine air responsible for many of the wind speed changes in the Mid-Columbia Basin. The 2-m to 80-m temperature difference and 10-m to 80-m wind shear define the vertical structure of the atmosphere below turbine level. They are more indicative of the diurnally driven variations in low-level wind speed and temperature profiles. The 80-m to 500-m wind shear and temperature

differences define the vertical structure of the atmosphere above turbine height and (during surges of marine air) within the marine layer. The 500-m to 1000-m wind shear and temperature differences define the vertical structure of the atmosphere near the top of the marine layer when marine air is present.

2.4 Description of Statistical Quantities Used to Evaluate Sensitivity

Three statistical quantities are used to qualify and quantify the relationship between the evaluation (IC) variables and correlation of those variables to the 80-m wind at the target location: sensitivity, frequency of significant sensitivity, and coefficient of determination (R^2). In this study, sensitivity is defined as the magnitude of the relationship between the IC variable and the forecasted metric variable at a later time.

Determining the true sensitivity would require a very large ensemble of perturbed NWP model simulations for which the ensemble spread is carefully managed to represent the true uncertainty of the forecast metric(s) and the IC variable states at each grid point. Obviously, the true sensitivity cannot be determined. However, it can be estimated by drawing from a sufficiently large sample (ensemble) of perturbed NWP model simulations for which the ensemble spread is adequately managed. Thus, for this study the sensitivity relationship is expressed as:

$$\frac{\partial F}{\partial s} = \frac{\text{cov}(F,s)}{\text{var}(s)} \quad (1)$$

where $\partial F/\partial s$ is defined as the sensitivity of a target forecast metric (F) to selected IC state variables from prior simulated times at all points in the model domain. The covariance (cov) and variance (var) are computed over all ensemble members (Ansell and Hakim 2007). Thus the sensitivity can be thought of as the slope of a linear relationship between the IC variable and the forecasted variable. A higher absolute sensitivity value means that a given change in the IC variable will lead to a larger change in the variable being forecasted.

While sensitivity gives some sense of how much the forecast metric typically changes for a given change in the IC state variable, it conveys no information on the strength and reliability of the relationship. In many cases where the IC state variable has a relatively low variance, the sensitivity can be high even when the relationship is weak. For this reason, the coefficient of determination (R^2) was used to measure how much of the variance can be explained by the linear relationship between the IC variable and the forecast metric. A high R^2 indicates that most of the variance can be explained by the relationship. Mathematically, R^2 is defined as follows:

$$R^2 = [\text{cov}(F,s)/(\text{var}(s) * \text{var}(F))] \quad (2)$$

Although a completely rigorous analysis of sensitivity R^2 values was beyond the scope of this study, previous research and model experiments have indicated that R^2 values in the 0.15 to 0.25 range represent significant and most likely predictable relationships, while R^2 values less than 0.1 represent sensitivity relationships that are weak and unlikely to be useful. For an R^2 value of 0.15, about 40% of the forecast error is explained, which can conservatively be considered to be

significant. R^2 values of 0.1 or less indicate that 30% or less of the forecast error is explained, which is not considered to be significant.

The frequency of statistically significant non-zero sensitivity helps to determine the usefulness of a given observation. At each time, a statistical test is employed to determine if there is sufficient confidence that the true sensitivity is non-zero as estimated using the 48-member ensemble. In this study, a given sensitivity is designated as “significant” if the confidence bounds are of the same sign at the 95% confidence level. Previous sensitivity research has shown that a 95% confidence interval is adequate in resolving high sensitive regions interest for synoptic flow (Torn and Hakim 2008).

Significant sensitivity can be aggregated over many times to compute the fraction of cases for which the sensitivity is significant. This quantity is determined at each grid point and compiled to create a map. A high percentage of significantly sensitive cases indicates that a strong and most likely predictable relationship truly exists in the data and is not an artifact of the ensemble sampling technique.

Sensitivities were computed from 48 ensemble members to determine the impact of an initial model state variable 1-hour and 3-hours ahead on the 80-m wind speed at Klondike, Stateline, and Hopkins Ridge. As mentioned earlier, the 1- and 3-hour look-ahead periods were chosen because they are of the most value to the grid operator.

In addition to raw sensitivity values, the R^2 values and significant sensitivity frequencies were computed for the 1- and 3-hour look-ahead times. The R^2 values were produced for each interval and then averaged over the entire 47-day sensitivity period. The frequency of significant sensitivity periods with a 95% confidence interval were produced for the entire 47-day sample.

In order to make inferences about the best measurement locations and variables to improve forecast performance over a wide variety of cases, it is necessary to construct a statistical composite of sensitivity values over a representative case sample. The simplest composite is an average, although other statistics may also be meaningful for a particular application.

In this study, the average was constructed for all dates and times in the analysis period to obtain information about which areas have the highest average sensitivity over all cases. In addition, the average was computed for each specific subset of the analysis period – such as those which experience large changes (ramps) in wind power production or time periods during which a particular wind or weather regime was present (such as northwest or southeast flow). This approach yields information about the locations and variables that have the most sensitivity for those types of events.

2.5 Location and Variable Combinations

The forecast sensitivity dataset can be used to select a combination of locations and variables that will provide the most improvement for the prediction of the forecast metric over the desired look-ahead period. Typically, the direct use of the most sensitive points would likely not yield an optimal solution because the IC variables, in general, have a significant degree of correlation. Even though a number of variables may exhibit a high degree of sensitivity, much of the “predictive” information in each variable is highly correlated with the information in other variables. Therefore, many of the highly sensitive variables/locations essentially provide redundant information about the variability of the forecast metric for a given look-ahead period.

In order to address this issue, the MOOA (Zack et al. 2010) was used to determine the relative predictive value of different combinations of variables/locations. In this procedure, a small set of variables/locations is selected by a separate algorithm and then multiple linear regression is performed on all combinations of variables/locations within that set. Unlike the study for Tehachapi Pass where the maximum average sensitivity magnitude was chosen (Zack et al. 2010), the locations of the maximum average R^2 value were chosen here for each IC variable considered. The maximum average R^2 value was chosen because it represents the goodness of fit for a linear regression and provides a better representation of the simulated sensitivity relationship than just the magnitude of average sensitivity.

The variables are normalized prior to the regression. The normalization permits the regression coefficients to be used as an indicator of the relative importance of each variable when combined with other variables in the set. The R^2 values of each multiple regression can also be used as an indicator of which combinations and individual variables/locations have the most value for a given forecast look-ahead period.

2.6 Regime-Based Sensitivities

Large wind ramps present a significant forecast challenge, since accurate prediction of both the timing and amplitude are important for grid operations. Furthermore, they are often caused by subtle features that are difficult to observe accurately. This study also attempts to address this issue by defining and analyzing the sensitivities for a period of observed wind ramp-events, referred to in this report as the ramp event subsample.

To examine IC variables that correlate to prediction of 80-m wind for wind ramp cases, the top ten up and down ramps in the region were compiled for each of the three sites for a total of 20 ramp events per site (Tables B1 through B3 in Appendix B). Tables 2 and 3 summarize the upward and downward ramp events for all three locations. The data were chosen from the generation and on-site met tower data provided by the grid system operator (Bonneville Power Administration). A power curve was used to estimate non-curtailed production. For this study, the subsample was composed of 20 ramp events for each site. Since some of the up and down ramps occurred within the same 3-hour interval, the number of events shown in Tables B1

through B3 ranges from 17 to 19 because these were the only unique 3-hour intervals for the cases. Event amplitudes were compared as a percent of plant capacity.

The upramp event amplitudes varied from 63.0% at Klondike to 98.7% at Stateline. The down ramp event amplitudes varied from -50.5 % at Stateline to -98.8 % at Hopkins Ridge. The durations ranged between 70 to 170 minutes for the upramps and from 70 to 220 minutes for the down ramps. These high impact ramp events are of particular interest because the locations and importance of the correlated IC variables for these events could not be represented well by the 47-day average results. When looking at the 47-day average, the high impact events will often be represented as outliers. Therefore, additional correlations were computed for the high impact ramp cases. Sensitivities computed for the ramp cases were then evaluated using the MOOA approach.

Table 2. Summary of upward ramp event for the three locations.

Wind Plant Location	Max Upramp % Cap	Min Upramp % Cap	Max 10-Min Upramp	Min 10-Min Upramp	Max Upramp Duration (Min)	Min Upramp Duration (Min)
Hopkins Ridge	98.2	86.4	66.4	17.5	130	90
Stateline	91.1	73.9	64.2	11.7	170	70
Klondike	76.0	63.0	70.3	9.2	120	70

Table 3. Summary of downward ramp event for the three locations.

Wind Plant Location	Max Down ramp % Cap	Min Down ramp % Cap	Max 10-Min Down ramp	Min 10-Min Down ramp	Max Down ramp Duration (Min)	Min Down ramp Duration (Min)
Hopkins Ridge	-98.8	-70.1	-30.8	-9.8	130	90
Stateline	-89.7	-50.5	-34.0	-6.4	220	70
Klondike	-74.6	-60.7	-65.8	-12.7	130	70

3. Single-Variable Results

This section discusses the spatial variation of sensitivity, R^2 , and frequency of significant sensitivity for a number of the variables listed in Table 1. Section 4 discusses the use of the MOOA technique to find optimal combinations of variables and locations.

3.1 Variation of Sensitivity by Time of Day

The flow in the Mid-Columbia Basin for the time period examined is more variable and influenced by mid-tropospheric, larger-scale patterns than for the Tehachapi Pass region (Zack et al. 2010). Large scale motions tend to have a higher day-to-day variability than the smaller scale (mesoscale) circulations in the Tehachapi Pass driven by terrain, land surface type, and sea

surface temperatures interacting with the diurnal cycle of heating and cooling.

Overall, the analysis indicates that the average Mid-Columbia Basin sensitivities are heavily influenced by the air being channeled eastward by the large-scale flow through the Mid-Columbia Basin and the profile of the low-level stability within the basin (Figure 2). Also, within the boundary layer, perturbations tend to amplify on the western front range of the Cascade Mountains as these features travel eastward toward the target location. The fact that more variable, large scale flows dominate the Washington-Oregon region seems to generate lower average sensitivities when compared to Tehachapi Pass.

The warm season sensitivity results for the Washington-Oregon region exhibited little significant diurnal variation in the sensitivity (not shown). This result was quite different from the warm season patterns in the Tehachapi Pass that were characterized by significant variations in the forecast sensitivity based on time of day (Zack et al. 2010).

The sensitivity results for the Mid-Columbia basin do show day-to-day variability in the locations and variables that have the greatest impact on the forecasts. Thus, the day-to-day variability is not very useful in directly meeting the primary object of this research, which is to identify measurement locations and variables that have the greatest positive impact on the accuracy of the 0- to 6-hour wind forecasts. However, as part of future research, an analysis that identifies flow regimes that make up the day-to-day variability could be useful in understanding how specific sensor deployment strategies impact forecasts for specific regimes.

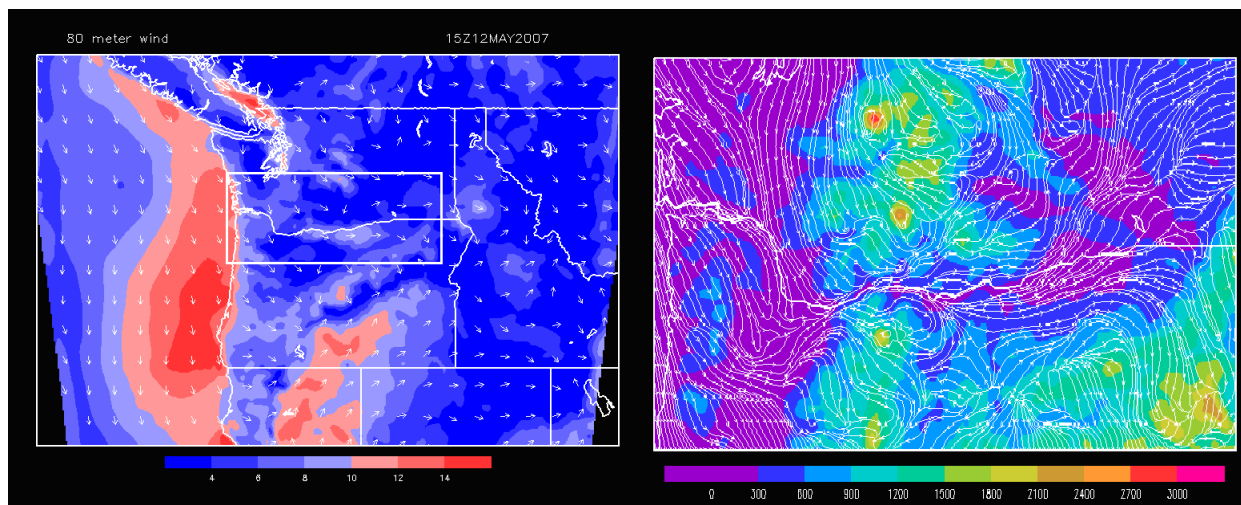


Figure 2. Left panel depicts the ensemble mean 80-m wind vectors and speed contoured for the outer domain. The right panel depicts the 80-m streamlines with terrain (color shading) for ensemble member number one on the inner grid over the Columbia Gorge (white box shown in the left panel). The right panel shows the 80-m flow being channeled eastward through the Mid-Columbia Basin. Both images are valid at 1500 UTC 12 May 2007.

3.2 Case Example

The output data from the ensemble of simulations provide a large volume of information about the space-time connection of atmospheric variability within the simulation domain. Figure 3 illustrates an example of data from all ensemble members and the resulting linear relationship for F, defined as the average 80-m wind speed in a rectangular area representing Hopkins Ridge for 0000 UTC 15 June 2007. In this case, the IC state variable is the 80-m wind speed three hours earlier at grid point (127, 85). Figure 2 indicates this as (127, 85), which is located to the southwest of the Hopkins Ridge target forecast area just to the east-southeast of Stateline (point A in Figure 5). Each data point denotes the value of the 80-m wind speed at grid point (127, 85) from 0000 UTC and the average 80-m wind speed in the Hopkins Ridge target area at 0300 UTC from one of the 48 ensemble members.

The plot indicates that there is a well-defined relationship between changes in 80-m wind speed for point (127, 85) at 0000 UTC and changes in the average 80-m wind speed over the forecast target area three hours later. The slope of the regression line through these points defines the sensitivity of the forecast metric to this specific IC variable and location for the date, time, and look-ahead period under consideration. The interpretation of the regression line is that a 1 m/s change in the 80-m wind speed at point (127, 85) is associated with a 1.15 m/s change in the 80-m wind speed in the Hopkins Ridge target area three hours later. The R^2 value for this regression is 0.429, which indicates that variation of the 80-m wind speed at 0000 UTC explains approximately 43% of the variance in the forecast target metric three hours later.

Another set of data from all ensemble members for the same date and time is shown in Figure 4. The forecast metric is the same (80-m wind speed in the Hopkins Ridge target area) but the IC state variable is the 80-m wind speed at a different model grid point (10, 98), which is denoted as point B in Figure 5. This point is located over the Pacific Ocean just about due west of Hopkins Ridge. The slope of the regression line associated with these data is essentially zero and the R^2 value is also approximately zero indicating the variable at this point for 0000 UTC explains none of the variance of the forecast metric three hours later at 0300 UTC.

A spatial representation of the sensitivity patterns for a particular date and time can be created by constructing a contour map of the sensitivity values (i.e. the slopes of the regression lines between each grid point and the target area). The map for 0300 UTC 15 June 2007 is shown in Figure 5. The forecast target region is represented by the white box. The map indicates that there is a region of high sensitivity in Oregon just south of the border to the southwest of Hopkins Ridge for this time period.

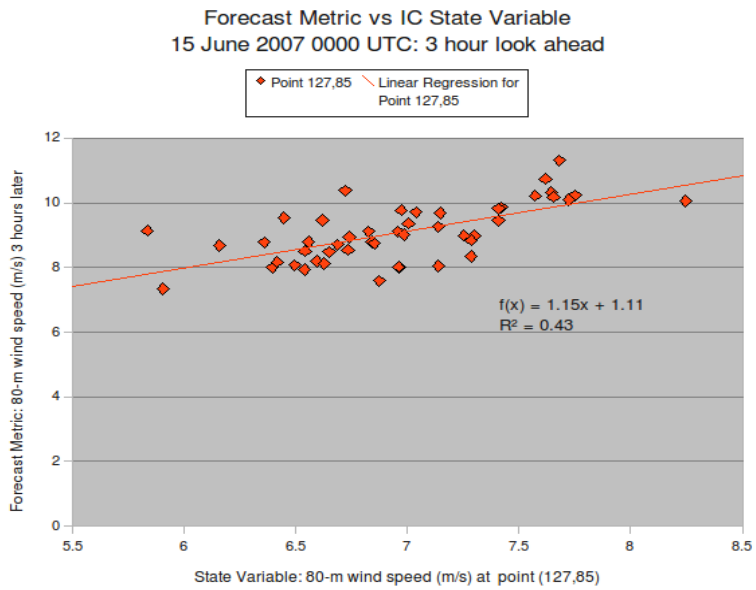


Figure 3. Scatter plot of an IC state variable (80-m wind speed) for model grid point (127, 85) at 0000 UTC 15 June 2007 versus a forecast metric (80-m wind speed) at 0300 UTC from each of the 48 ensemble members and the associated regression line.

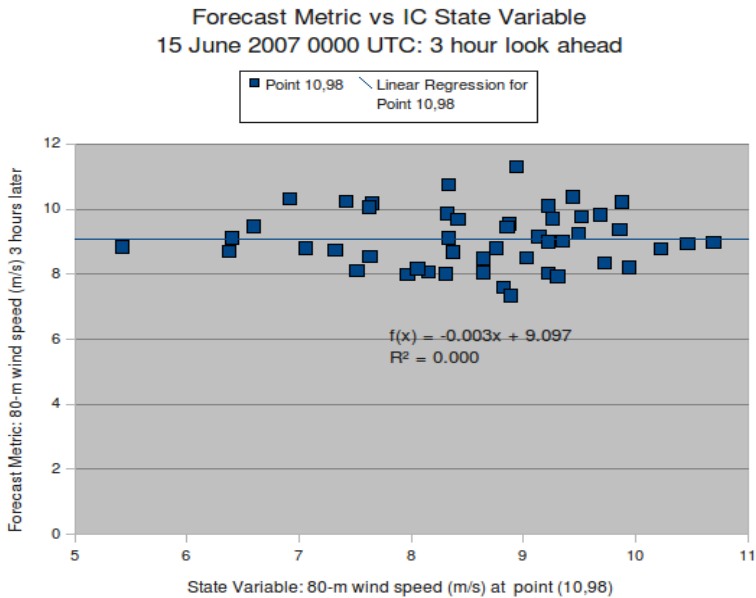


Figure 4. Scatter plot of an IC state variable (80-m wind speed) for model grid point (10, 98) at 0000 UTC 15 June 2007 versus a forecast metric (80-m wind speed) at 0300 UTC from each of the 48 ensemble members and the associated regression line.

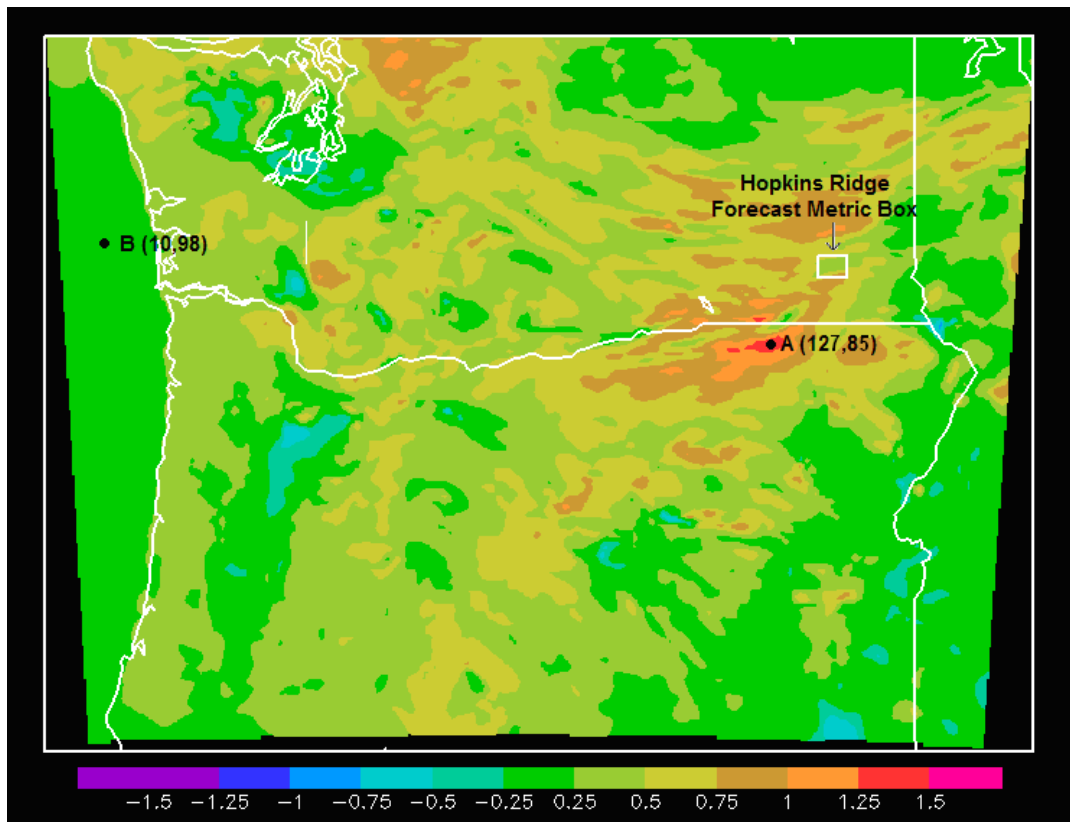


Figure 5. Forecast sensitivity of the average 80-m wind speed in the white box (forecast metric box) at 0300 UTC 15 June 2007 to 80-m wind speed three hours earlier with areas of high (point A) and low (point B) sensitivity marked.

3.3 Climatology of Sensitivity

In order to make inferences about the best measurement locations and variables to improve forecast performance over a wide variety of cases, it is necessary to analyze a statistical composite of sensitivity values over a representative sample of cases. Two analyses were performed. One analysis includes all cases while the other was done on a subsample of cases that only included large ramps in wind power production.

The average sensitivities, R^2 values, and frequency of significant sensitivities were computed over all time periods in the 47-day analysis period for several selected IC variables for Hopkins Ridge, Klondike and Stateline. The area of maximum R^2 (Fig. 14 and Appendix F) and sensitivity values (Figs. 7-13 and Appendices D and E) varies from site to site, but the parameters show the same general magnitude regardless of the metric location, suggesting that these results may be useful at all rather than one specific location. This result was most evident in R^2 values of 80-m wind sensitivity at various metric sites for the 3-hour look ahead period which all show maximum R^2 values ~ 0.15 in close proximity to the target regions (Figures F12, F14, F18).

3.3.1 Look-Ahead Time Sensitivities

The average 47-day sensitivity values of 80-m wind speed in the target box to 80-m wind speed for 1-hour look-ahead period are shown in Figure 6. The highest sensitivity values for the 1-hour look-ahead time are in close proximity to the metric location while the 3-hour look-ahead time (Fig. 7) shows the highest sensitivity values located further upstream (to the southwest). However, the magnitude of the maximum sensitivity, however, is lower at the 3-hour look-ahead time (note the different scales in Figs. 6 and 7).

For the 47-day average, there was a similar decrease in magnitude of R^2 and maximum R^2 with increasing look-ahead time and distance from the forecast site (not shown). The high 1-hour look-ahead sensitivities and R^2 values for 80-m wind speed very close to the target location shows that for average forecast skill, persistence tends to dominate as the best forecast method at very short lead times. This relationship between forecast skill and persistence is not true for ramp events as discussed in section 4. As the look-ahead time increases, correlations between the IC parameter and the metric parameter tend to decrease with the area of maximum correlation typically farther upstream.

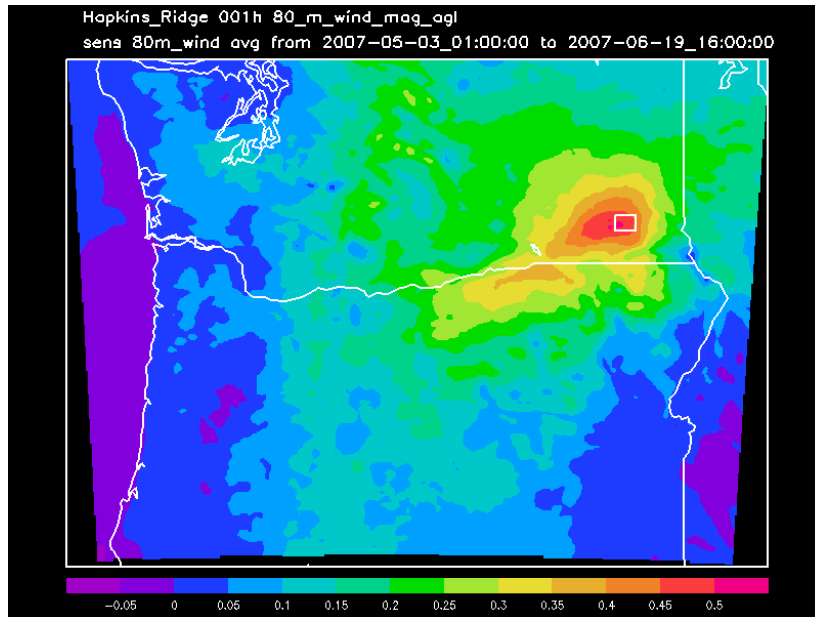


Figure 6. Average sensitivity of 80-m wind speed (m/s) within the white target box to 80-m wind speed (m/s) throughout the entire grid domain for a 1-hour ahead forecast for all time periods in the 47-day analysis period for Hopkins Ridge.

3.3.2 Site-to-Site Sensitivity Variability

The variability of the sensitivity patterns from site to site can vary widely depending on which IC variable was used in the sensitivity calculations. The sensitivity of 80-meter wind speed at each target location to the variation of 80-m wind speed 3 hours earlier at all grid points are shown in Figures 7 through 9. An area of high sensitivity values located just south of the Mid-Columbia Basin in northern Oregon is present for all target locations. This relationship between the wind speed at the target location and the wind speed three hours earlier along the Mid-Columbia Basin has the highest magnitude relationship for the Klondike location as shown in Figure 9. For a 1 m/s increase in wind speed within the area of maximum sensitivity for Klondike, there will be 0.5 m/s increase 3 hours later at the Klondike target location.

A second area of increased sensitivity values are located parallel to the Cascade Range running from north central Washington toward the south through Oregon. This area of high sensitivity corresponds with the region of higher 80-m wind speeds shown in Figure 2 where eastward-flowing marine air exiting the Columbia Gorge is still channeled by somewhat higher terrain to the north and south. For such a high magnitude sensitivity to exist, there has to be enough spread (uncertainty in the true initial state) in the IC and metric variables to account for it, especially if R^2 is not small, as is the case here (not shown).

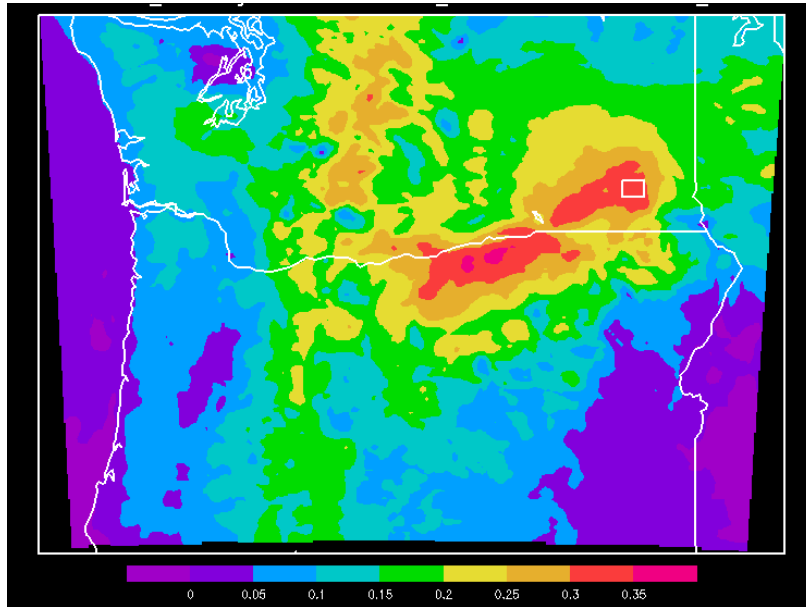


Figure 7. Average sensitivity of 80-m wind speed (m/s) within the white target box to 80-m wind speed (m/s) throughout the entire grid domain for a 3-hour ahead forecast for all time periods in the 47-day analysis period for Hopkins Ridge. Note that the scale extends from 0 to 0.35.

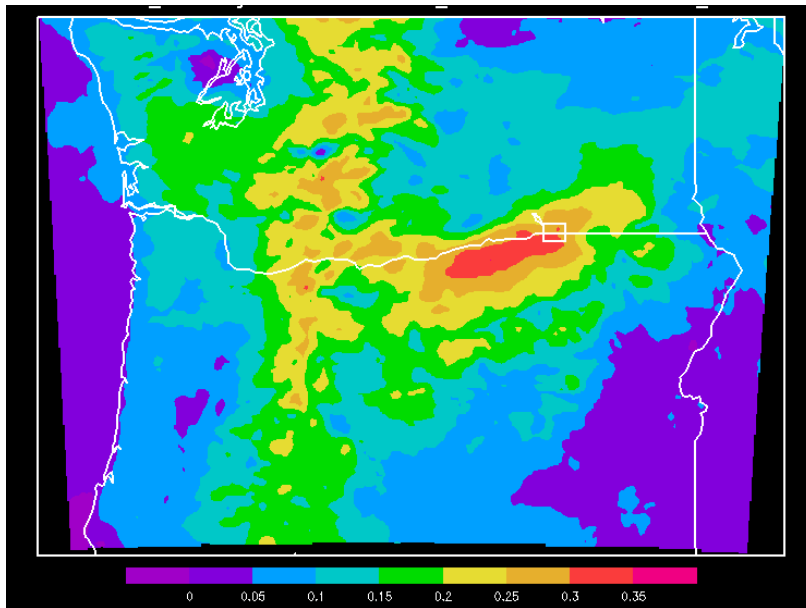


Figure 8. Average sensitivity of 80-m wind speed (m/s) within the white target box to 80-m wind speed (m/s) throughout the entire grid domain for a 3-hour ahead forecast for all time periods in the 47-day analysis period for Stateline. Note that the scale extends from 0 to 0.35.

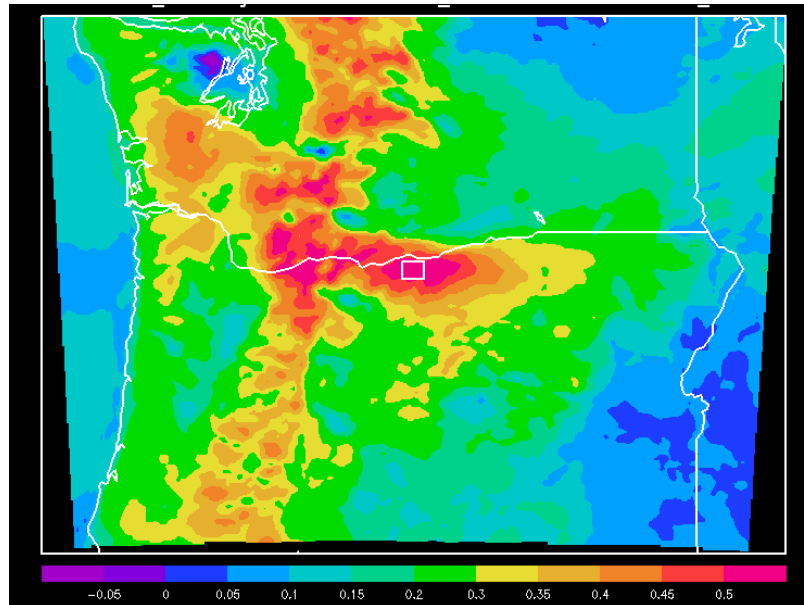


Figure 9. Average sensitivity of 80-m wind speed (m/s) within the white target box to 80-m wind speed (m/s) throughout the entire grid domain for a 3-hour ahead forecast for all time periods in the 47-day analysis period for Klondike. Note that the scale extends from -0.05 to 0.5.

3.3.3 Sensitivity of Different IC Parameters

To determine the impact of other variables on wind speed at the target locations, the twelve IC parameters listed in section 2.3 were examined for all three metric locations. This subsection examines how sensitivity varies among variables.

Similar to the Tehachapi region results (Zach et al. 2010), winds at 80 m seemed useful to predict the wind speed at the 80-m level within the target location at a later time. Sensitivities were also computed for 250-m AGL wind speed, 1.5-km AMSL wind speed and 3-km AMSL wind speed for the three target locations. At the lowest level, 250-m wind speeds produced almost identical results to that from the 80-m level, with the maximum sensitivities being slightly lower in magnitude (not shown). For winds higher up in the atmosphere, the sensitivity pattern converged along the Cascade Range, as shown in Figure 10 for Hopkins Ridge for the 3-km level. Even though sensitivity values are lower for this level, the higher terrain to the west (i.e. upstream in the seasonal climatological flow) is an area of increased uncertainty in the simulations.

As seen in the previous results for the Tehachapi region (Zack et al. 2010), levels far above the turbine height can yield useful statistical relationships. Therefore, the role of wind speed change with height (i.e. wind shear) was examined as an IC parameter for the three layers listed in Table 1 (10-m to 80-m AGL, 80-m to 500-m AGL, 500-m to 1-km AGL). The greatest sensitivity

values over a large area were obtained by examining the 10-m to 80-m AGL layer that is just below turbine height. Results for this layer at Klondike are shown in Figure 11 while those for Stateline and Hopkins Ridge are presented in Appendix D (Figs. D3 and D4). The area of highest sensitivity is located to the east of Klondike along the Mid-Columbia Basin.

When wind shear is high below the turbine height, the wind speed at the turbine height is almost certain to be high as well. This increase in wind speed may be fueled by cooling of the 2-m surface temperatures just upstream of the Klondike location at higher elevations, which can lead to downslope flow toward the target location. This situation is illustrated in Figure 12 by negative sensitivity values to 2-m temperature just to the west of the Klondike metric location in the higher terrain of the Cascade Range.

Above the surface layer, there is also an enhanced region of higher sensitivity values for the 2-m to 80-m temperature difference IC parameter (Figure 13 and D7 and D8 in Appendix D). This area of enhanced sensitivity is collocated with the increased values in low-level wind shear sensitivities (for Klondike). For regions of highest sensitivity, a strong decrease in temperature with height near and just below the turbine height is correlated to an increase in the Klondike wind speed 3 hours later. The plausible mechanisms for increasing wind speed at the target location are horizontal transport as well as mixing of higher momentum air downward from air above the turbine height. Strong cooling above the turbine layer or warming below the turbine layer would help facilitate vertical mixing and increase wind speeds within the target location.

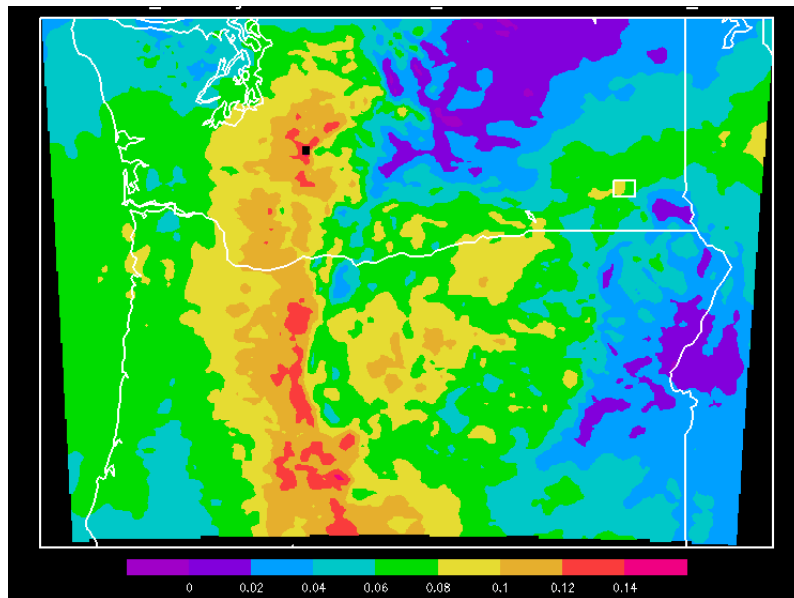


Figure 10. Average sensitivity of 80-m wind speed (m/s) within the white target box to 3-km AMSL wind speed (m/s) throughout the entire grid domain for a 3-hour ahead forecast for all time periods in the 47-day analysis period for Hopkins Ridge. Note that the scale extends from 0 to 0.14.

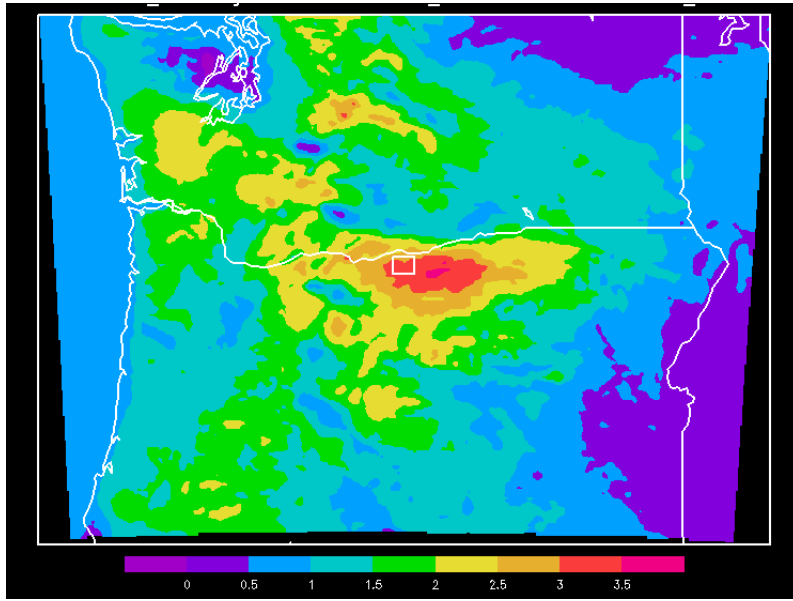


Figure 11. Average sensitivity of 80-m wind speed (m/s) within the white target box to 10-m to 80-m AGL wind shear throughout the entire grid domain for a 3-hour ahead forecast for all time periods in the 47-day analysis period for Klondike. Note that the scale extends from 0 to 3.5.

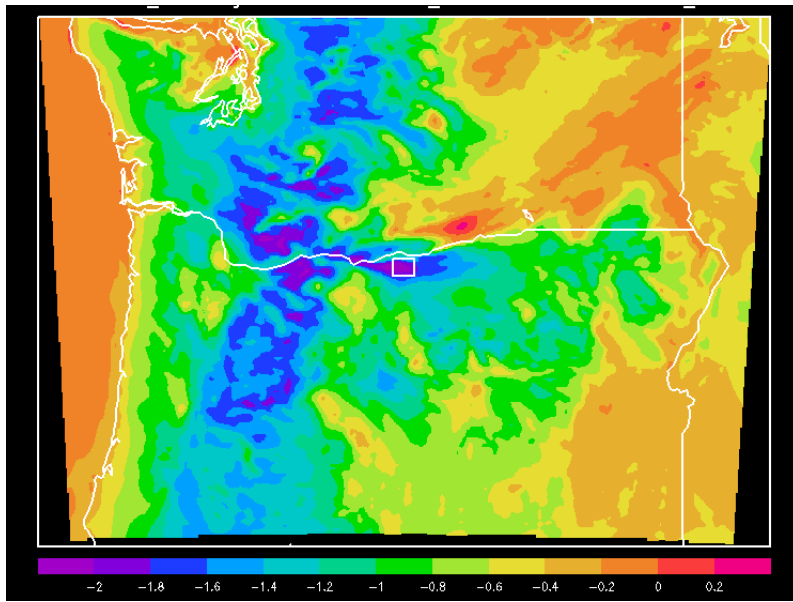


Figure 12. Average sensitivity of 80-m wind speed (m/s) within the white target box to 2-m temperature throughout the entire grid domain for a 3-hour ahead forecast for all time periods in the 47-day analysis period for Klondike. Note that the scale extends from -2 to 0.2.

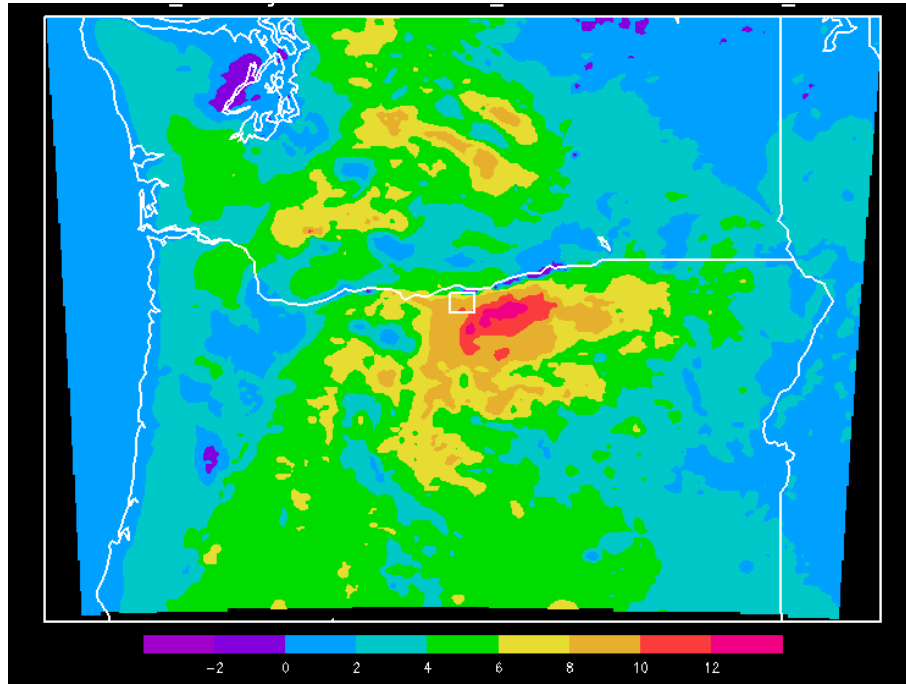


Figure 13. Average sensitivity of 80-m wind speed (m/s) within the white target box to 2-m to 80-m temperature difference throughout the entire grid domain for a 3-hour ahead forecast for all time periods in the 47-day analysis period for Klondike. Note that the scale extends from -2 to 12.

The vertical temperature gradient sensitivities were also examined for 80-m to 500-m AGL, 500-m to 1-km AGL and 80-m to 1-km AGL. These IC variables as well as some of the wind shear IC variables did not produce any obvious regions of high sensitivity or produced regions of the highest sensitivity that were located far from the target location. Figure E1 (Appendix E, lower left) shows areas closest to the target location produced low sensitivities of 80-m wind to the 80-m to 1-km AGL temperature gradient. Areas along the southern boundary showed high sensitivity that is likely related to boundary perturbations rather than physical processes correlated with the target region. There were some areas of moderate sensitivity that could be physically correlated to the target site located far from the metric location. An example in Figure D1 shows the 3-km wind speed sensitivities to the 80-m wind speed for the Hopkins Ridge target area.

The sensitivities to the 80-m wind speed for other target locations and IC variables, such as vertical wind shear, vertical temperature difference and temperature listed in Table 1 are provided in Appendix D. Overall, sensitivities with the best results were obtained from the lowest levels of the atmosphere for vertical gradient changes (wind speed and temperature). These parameters were chosen for use in the MOOA as discussed in Section 4.

3.3.4 Coefficient of Determination (R^2) Analysis

Similar to a map of sensitivities (e.g. Fig. 9), R^2 can be plotted for the entire region as well (Fig. 14). The average value of the sensitivity relationship for 80-m wind speed (Fig. 9) at every grid

point for all 47 days shows the regions of high sensitivity and high R^2 are, for the most part, collocated. However, some regions of high sensitivity east of the metric location have somewhat lower R^2 . Since R^2 is a measure of the amount of variance in the forecast metric that is explained by the relationship, it is hypothesized that as long as the magnitude of the sensitivity can be measured in the region of highest R^2 values, these locations will most likely contribute useful information to the model initial state and subsequently improve the forecast performance of 80-m wind speeds 3 hours later at the target location. Therefore, areas of high R^2 values can be good candidate locations for future atmospheric observations. These locations were examined in more detail using the MOOA methodology discussed in Section 4 to determine the best combinations of observations and locations that would most improve the forecast of 80-m wind speed.

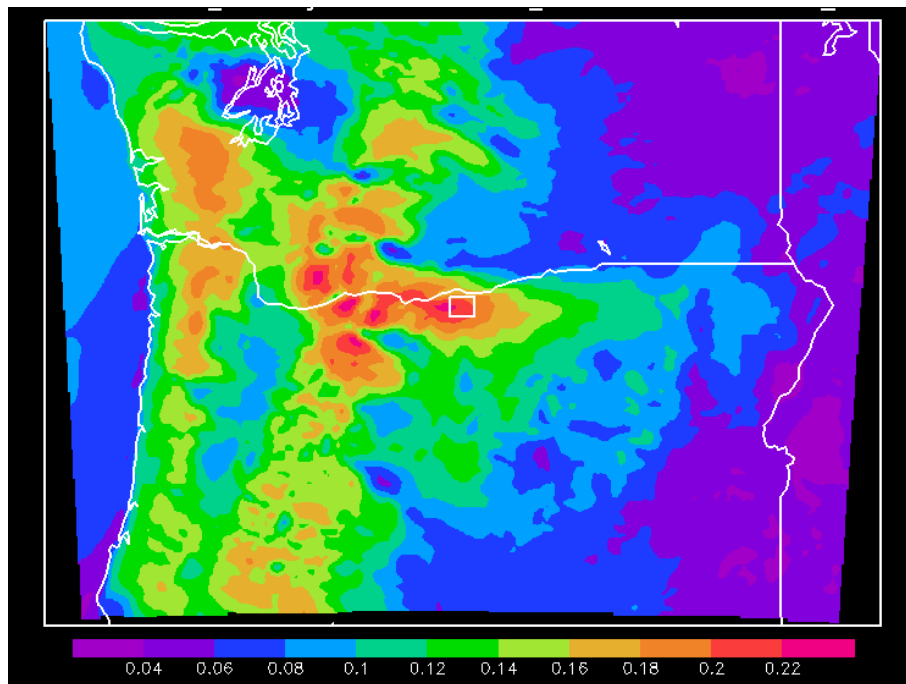


Figure 14. Average R^2 of the sensitivity of 80-m wind speed (m/s) within the white target box to 80-m wind speed throughout the entire grid domain for a 3-hour ahead forecast for all time periods in the 47-day analysis period for Klondike. Note that the scale extends from 0 to 0.22.

3.3.5 Significant Sensitivities

As noted earlier, an alternative summary statistic is the frequency with which an IC variable exhibits statistically significant non-zero sensitivity at the 95% confidence level. If this criterion is satisfied for a specific grid point and time, it indicates only a 5% probability that the sensitivity was produced by random data variations drawn from a sample in which the actual sensitivity was zero or of a different sign than the estimated sensitivity. Thus it is very unlikely that the actual sensitivity is zero or of a different sign at that point and time. However, this statistic does not provide information about the magnitude of the sensitivity.

For the Mid-Columbia Basin, the statistically significant non-zero sensitivity at the 95% confidence level was computed for each forecast interval in the 47-day analysis sample. Then the fraction of the 47-day sample having non-zero sensitivity was calculated for each of the IC variables under considerations.

Figure 15 illustrates the frequency of statistically significant non-zero sensitivity to the 80-m wind for a 3-hour forecast of the average 80-m wind speed in the metric area (white box) for the Hopkins Ridge location. This plot is similar to Figure 7 but for statistically significant sensitivities with a 95% confidence interval instead of raw sensitivity values. The frequency is over 50% for the points within the metric box itself and the area of greater than 45% frequency extends along the eastern half of Washington southwest to the Mid-Columbia Basin. The highest frequency of around 50% is in the immediate vicinity of the metric box itself. The fact that the area in the vicinity of the metric box has a high frequency of statistically significant non-zero sensitivity but a somewhat smaller average sensitivity (Figure 7) suggests that the 80-m winds in metric box have a very persistent, but smaller sensitivity to the local values 3 hour earlier, while sensitivities to the west are stronger, but less consistent.

This result is consistent with the fact that the recent history of the winds in the vicinity of the wind generation facility typically has, on average, the most predictive value. The off-site locations to the southwest along the Mid-Columbia Basin have a much higher average sensitivity (Figure 7) and the frequency of statistically significant non-zero sensitivity is modestly lower near 45%. At this location, offsite data may be highly useful in a subset of cases. The combination of high average sensitivity and high frequency of non-zero sensitivity make these among the best locations for additional measurements to improve the forecasts at the Hopkins Ridge location.

Similar results were obtained for Klondike, highlighting an area of interest along the Mid-Columbia Basin in Northern Oregon (Fig. 16). The locations of largest statistically significant sensitivities were within the metric area for Klondike. The sensitivity values for Klondike are greater than those for Hopkins Ridge, which could be useful in determining where to place observation sites. The fact that the Klondike sensitivity values are larger than those for Hopkins Ridge gives greater confidence that 3-hour forecasts for Klondike would benefit from added observations in the more frequently sensitive area.

The plots of significant sensitivities typically feature spatial patterns that are more similar to R^2 than average sensitivities. However, the 80-m wind speed results for Klondike are an exception as both significant (Fig. 16) and average sensitivity (Fig. 9) show large values east of the metric box, while average R^2 (Fig. 14) does not. This result implies that R^2 is much higher to the west of the metric location at Klondike than the value used to compute the 95% confidence threshold for significant sensitivities.

When the highest average and significant sensitivities do not overlap in a given region, it indicates that, in the area of highest average sensitivity, a small change in the IC value can be correlated to a relatively large change in wind speed 3 hours later at the metric location. But, the area of high average sensitivity values can be neither common nor of a magnitude that is

statistically significant for that sample.

An example of this scenario is shown by comparing areas for Hopkins Ridge in Figures 7 and 15. The region of maximum significant sensitivity is located just southeast of the metric location, while the highest magnitude average sensitivity values are located far to the southwest along the Mid-Columbia Basin. This spatial disconnect may be due to the impact of outlier events on the average sensitivity values. Because average values can be affected by outlier data, they produce high sensitivities even though the high sensitivity values are uncommon (and hence not statistically significant at the 95% confidence level). On the other hand, significant sensitivities weigh each period with the same magnitude, regardless of the magnitude of the sensitivity. Therefore, outlier events do not affect the significant sensitivity results and the most frequent relationship is revealed.

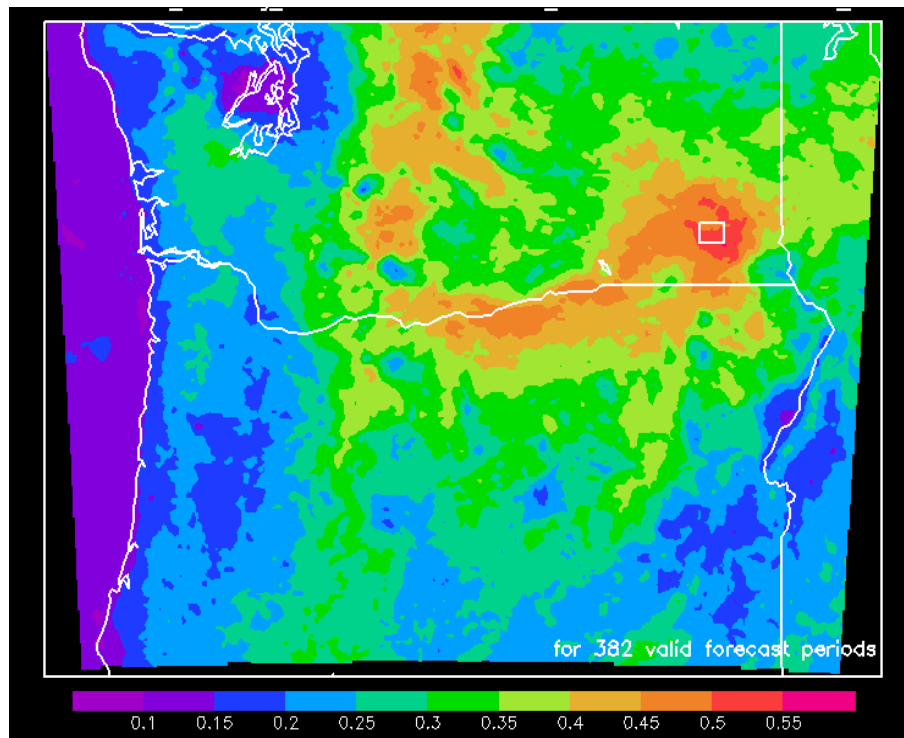


Figure 15. Frequency (fraction of time periods) of statistically significant non-zero sensitivity at the 95% confidence level of the average 80-m wind speed in the forecast metric area (white box) for Hopkins Ridge to 80-m wind speed 3 hours earlier for the 47-day sample.

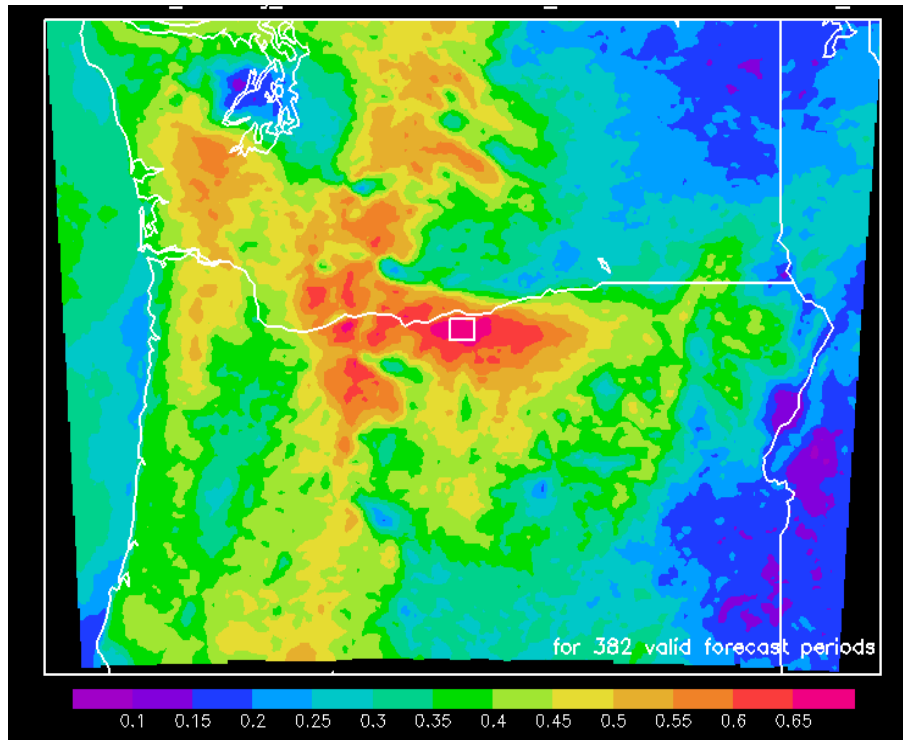


Figure 16. Frequency (fraction of time periods) of statistically significant non-zero sensitivity at the 95% confidence level of the average 80-m wind speed in the forecast metric area (white box) for Klondike to 80-m wind speed 3 hours earlier for the 47-day sample.

3.3.6 All Case Summary

Correlation parameters for 80-m wind speed, 2-m to 80-m temperature gradient, and 10-m to 80-m wind shear show the best results; therefore these parameters should provide the maximum improvements to short-range forecasts at the target locations. Results from this section show that additional observations in a region extending from the Columbia Gorge eastward through the Mid-Columbia Basin would be the most valuable in improving the short-term forecast at the target locations. The Klondike site showed higher magnitudes of sensitivity, R^2 and frequency of significant sensitivity than the other locations.

It is hypothesized that these three parameters help the model to accurately simulate the impacts of the advection of 80-m wind speed and vertical mixing from wind shear and vertical temperature gradient on turbine-level wind speeds. The IC variables not used were those that produced inconsistent sensitivity results such as low values near the metric location or high values located much farther away.

The correlation statistics give the most unambiguous results as to the predictive relationship of a given variable for the target location. To determine if one location could improve the forecast at multiple metric locations, similarities between the sensitivity fields and R^2 values for different metric locations must be examined. The most notable location where this occurred was within

the lower elevations along the Mid-Columbia Basin, which had increased 80-m wind speed sensitivities to several target locations. For example, Figures 8 and 9 show very similar sensitivity patterns for Stateline and Klondike. The 80-m wind speed sensitivities for Hopkins Ridge shown in Figure 7 were also quite similar. Even though there are some differences between sensitivity fields, the southern edge of the Mid-Columbia Basin (for all sites) and parts of Eastern Washington State (for Stateline and Hopkins Ridge) are potentially very important locations for wind measurements.

Figure 17 compares the 10-m to 80-m wind shear plots of Stateline and Hopkins Ridge, while Figure 11 shows the same parameter for Klondike. The regions of high sensitivity are generally in the same area for Stateline, Klondike and Hopkins Ridge, indicating that a single observing location could improve forecasts for all three sites. This simulated relationship should be tested over a larger sample that includes all seasons and, if possible, validated using available observations to determine the potential value of additional sensors in the region.

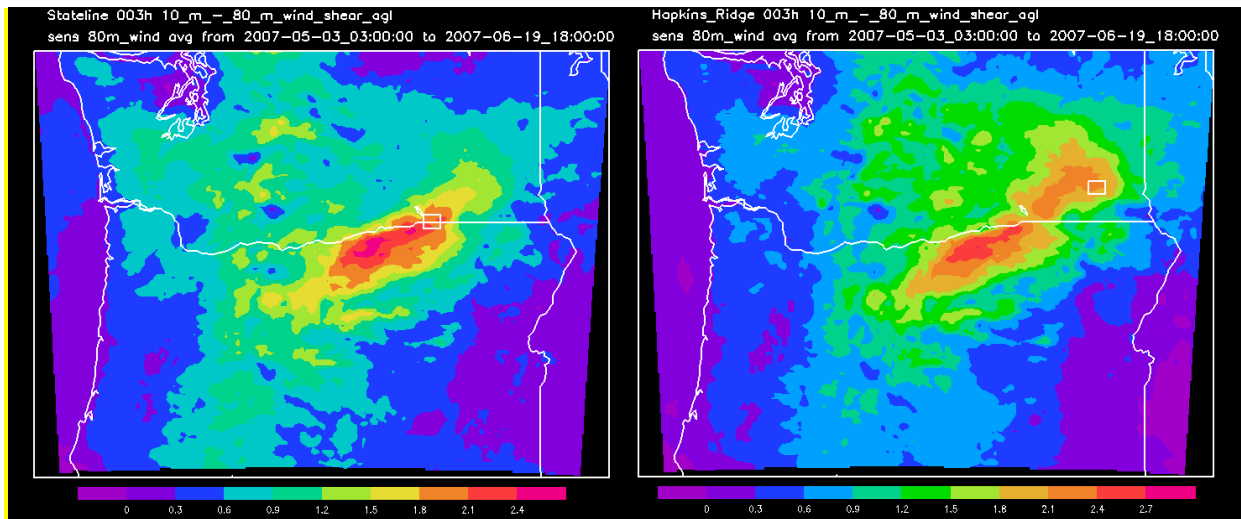


Figure 17. Average sensitivity of 80-m wind speed (m/s) within the white target box to 10-m to 80-m AGL wind shear throughout the entire grid domain for a 3-hour ahead forecast for all time periods in the 47-day analysis period for Stateline (left) and Hopkins Ridge (right).

4. Multiple Variable Results

Section 3 discussed the spatial variation of sensitivity and several statistical quantities used to identify the most useful locations over the 47-day period. This section explores techniques to identify the best combination of variables and locations to achieve maximum reduction in forecast error.

MOOA was applied to the forecast sensitivity data generated for the Mid-Columbia Basin. Separate calculations were performed for the full 47-day sample and the ramp-event subsample described in section 2.6.

Of the twelve variables listed in Table 1, only 80-m AGL wind speed, 2-m to 80-m AGL temperature difference, and 10-m to 80-m AGL wind shear were chosen for use in the MOOA regression method. These variables were selected because: (1) they showed the largest maximum R^2 values and frequency of significant sensitivity for all three forecast locations, and (2) visually the largest R^2 values were located near or upstream of the forecast sites. Also, it was important that the location of largest R^2 values overlap with non-zero values of sensitivity, implying physical and not just statistical correlation with the metric variable.

For multivariate regression, the locations for each variable were chosen using the maximum average R^2 during the period over which the MOOA was applied to either the full or ramp subset period. Plots of R^2 values used to pick the locations in the multivariate regression are shown in Appendix F. An example where areas of increased R^2 do not overlap with highest sensitivity is shown by comparing Figures E1 (Appendix E, bottom left) and F22 (Appendix F).

Only one wind speed level was selected due to the likely high degree of correlation between them, and because of computational limits in applying MOOA to multiple variables. The 2-m AGL temperature showed R^2 values that were only slightly lower than those of the three included variables for Klondike and Stateline. However, regions of significant R^2 were located significantly farther away from the forecast metric site than the other three variables along the crest of the Cascade Range as shown in Appendix F Figures F13, F17 and F21. It would be challenging to measure representative 2-m temperature at these locations in complex terrain. More importantly, the large separation distance suggests that 2-m temperature sensitivity at these points is correlated but not physically linked to the forecast metric in the regions of interest. Measurements of 2-m temperature or other variables with similar relationships would not likely improve forecasts of the target metric when assimilated directly into NWP models.

In general, the locations of maximum average R^2 values are somewhat different for all cases and the ramp subsample (Figs. 18 through 20). The 80-m wind observation and wind shear maximum R^2 values are usually near the metric box for both samples and three locations, while the lapse rate measurement is usually in higher terrain upstream or to the west of the metric location.

Once this set of variables/locations was determined (Figs. 18 through 20), multiple linear regression was performed on all combinations of variables/locations separately for the full sample and ramp event subsample. The R^2 values for the resulting regression equations for each

site are listed in Tables 5 through 7. Among the single variable regressions for the full period averages, the 80-m wind speed had the highest R^2 value for all sites except Stateline, indicating that this variable is most likely the best single quantity to measure at that location. The results at Stateline suggest that a quantity involving any low-level wind information could be equally helpful, since the 80-m wind speed has a slightly lower R^2 value than shear.

However, the R^2 values for the other two single variable regressions were only modestly lower, which suggests that they might add additional predictive value. The ramp subsample for these sites showed that wind shear and the vertical temperature gradient become increasingly important for all sites except Stateline. Therefore, the value in measuring multiple variables depends on the period being examined, suggesting that a regime-based study could help to quantify these results.

As in previous efforts focused on the Tehachapi region (Zack et al. 2010), all two-variable regressions had a substantially higher R^2 value than the best single variable regression. For the most part, no two-variable observation combinations produced significantly higher R^2 than the other combinations. The one exception is Stateline, where the 80-m wind speed and 10-m to 80-m shear offer somewhat higher R^2 , especially for all periods. The results from the three-variable regressions indicate additional value – using all three variables yielded a higher R^2 than only two except at Stateline for all periods and Hopkins Ridge for ramp periods.

In addition to R^2 values, the actual magnitudes of the normalized coefficient values were examined to determine the importance of each variable. Table 8 shows these coefficient values for the regression at Klondike using the three variables discussed previously. In the Klondike region for the general average 47-day correlations, 80-m wind speed has the highest coefficient value implying that it is the most important for the general sample to predict 80-m wind speed at the target location. On the other hand, 2-m to 80-m temperature lapse rate has the lowest coefficient value of 0.037 meaning it may not provide much additional information when observations of all three variables are available.

For the ramp case statistics, the coefficient for Klondike 2-m to 80-m temperature lapse rate increases substantially from the 47-day average value (Table 8). The 10-m to 80-m wind shear coefficient also increases from 0.251 for the 47-day average to 0.284 for the ramp event average while the 80-m wind speed coefficient decreases from 0.260 to 0.095. These results suggest that for ramp events, vertical processes play a much more important role, and added observations of vertical temperature and wind speed gradients become increasingly useful in the prediction of wind speed at the target location. The ramp regime results suggest that computing sensitivity statistics for additional carefully defined regimes may identify additional valuable observing sites.

The results in Table 5 only represent the average R^2 for all the time periods in the respective sample. However, the R^2 values actually vary substantially among the ramp sample time periods from a high of about 0.8 to a low of slightly under 0.02 (Figure 21). A similar degree of variability was found in the full 47-day sample. Thus, it is evident that the forecast metric is substantially more sensitive to this combination of variables/locations for some time periods than

others.

In addition to variability in the three-variable R^2 values within the ramp-event sample (Figure 21), there was also a considerable amount of variability in the relative contributions of each variable at its location of maximum R^2 (Figure 22). As noted earlier, the variables have been normalized, so the magnitude of the coefficients is a direct indication of the relative influence of each variable on the overall relationship.

It is evident that all three IC variables show substantial variation in R^2 among cases. Furthermore, R^2 varied significantly between cases depending on IC variable suggesting that different variables are important in different cases. For example, vertical processes may be important in cases with large R^2 for wind shear or vertical temperature difference while horizontal processes may be important when R^2 for 80-m wind speed is large. As a result, the best IC variables/locations to observe for one type of ramp event could be different from those for another type of event. Breaking out ramp events into several regimes based on the triggering mechanism may provide additional value. This approach would require selecting a lower threshold for ramp amplitude in order to provide a larger sample size.

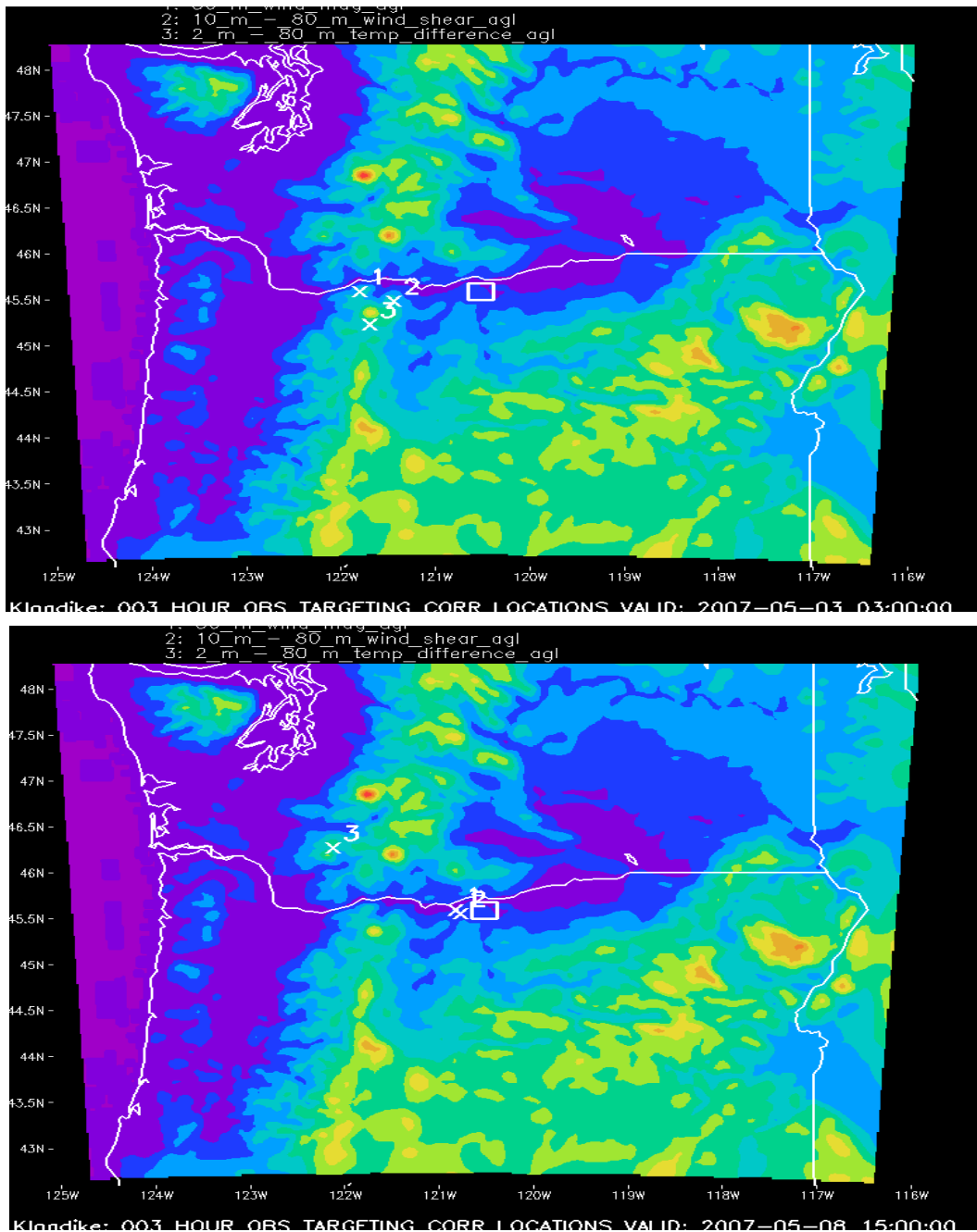


Figure 18. Points of maximum average 47-day (top) and ramp subset (bottom) R^2 sensitivity for a 3-hour forecast of the average 80-m wind speed over the Klondike target area (white box) for three IC variables: (1) 80-m wind speed, (2) 10-m to 80-m wind shear, and (3) 2-m to 80-m temperature difference. The color shading depicts the elevation (m) of the model terrain above sea level.

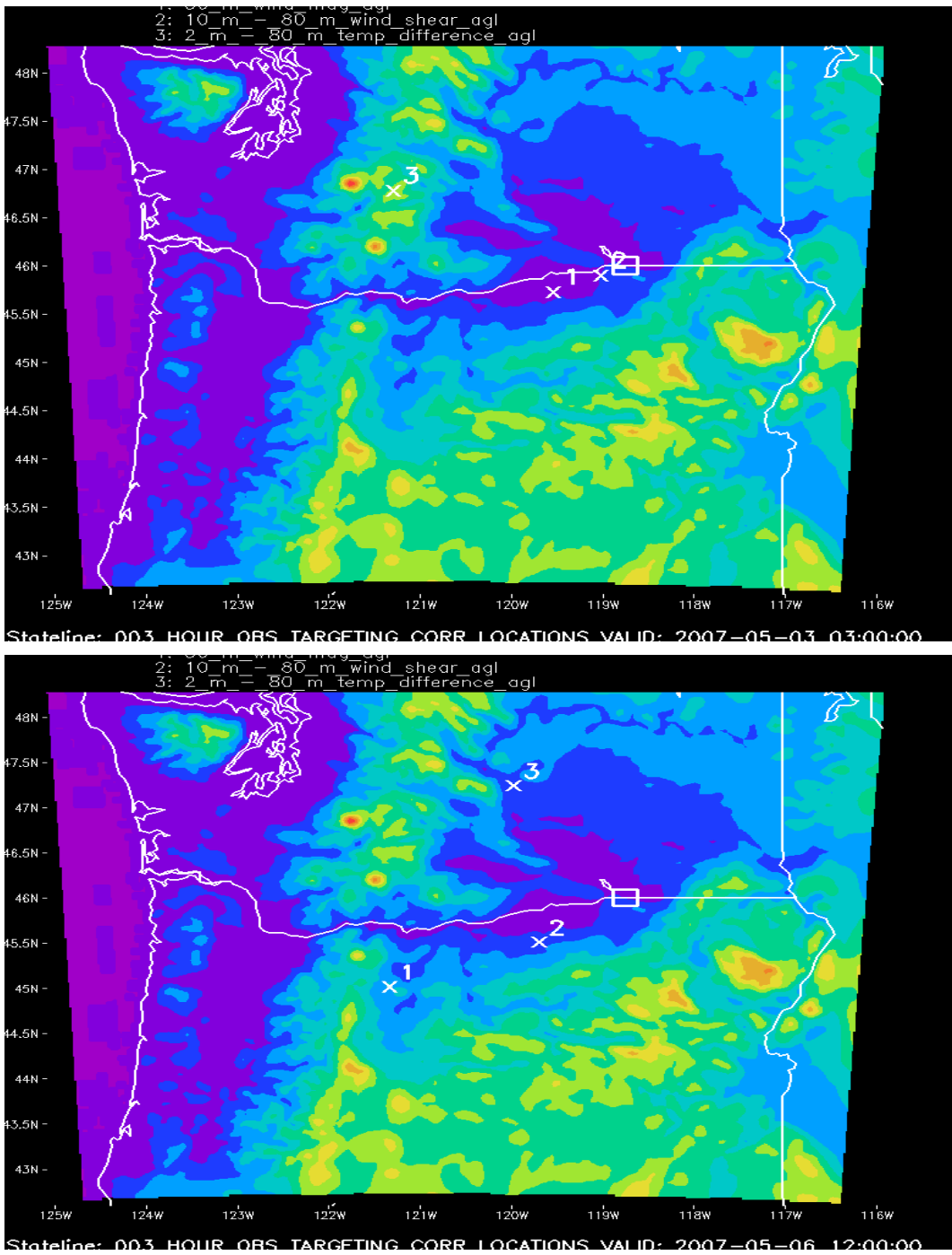


Figure 19. Points of maximum average 47-day (top) and ramp subset (bottom) R^2 sensitivity for a 3-hour forecast of the average 80-m wind speed over the Stateline target area (white box) for three IC variables: (1) 80-m wind speed, (2) 10-m to 80-m wind shear, and (3) 2-m to 80-m temperature difference. The color shading depicts the elevation (m) of the model terrain above sea level.

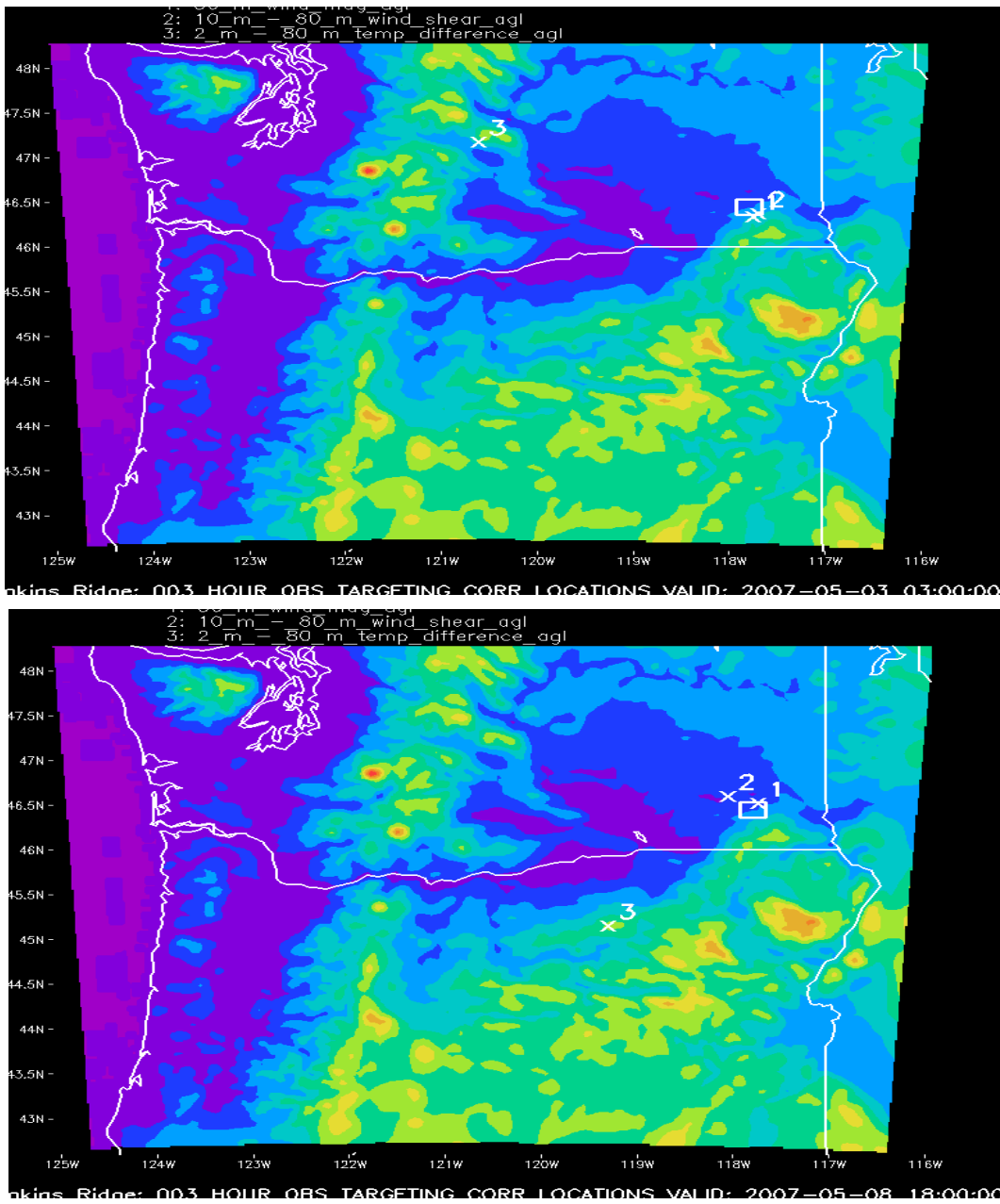


Figure 20. Points of maximum average 47-day (top) and ramp subset (bottom) R^2 sensitivity for a 3-hour forecast of the average 80-m wind speed over the Hopkins Ridge target area (white box) for three IC variables: (1) 80-m wind speed, (2) 10-m to 80-m wind shear, and (3) 2-m to 80-m temperature difference. The color shading depicts the elevation (m) of the model terrain above sea level.

Table 5. Average R^2 value for 1-, 2-, and 3-variable sensitivity regression for a 3-hour forecast of 80-m wind speed in the Klondike target area for all time periods and only ramp periods.

IC Variables	All Periods	Ramp Periods
One Variable		
(1) 80-m wind speed	0.305	0.302
(2) 10-m to 80-m wind shear	0.294	0.314
(3) 2-m to 80-m temperature difference	0.249	0.258
Two Variables		
(1) and (2)	0.359	0.346
(1) and (3)	0.349	0.370
(2) and (3)	0.348	0.383
Three Variables		
(1), (2) and (3)	0.395	0.411

Table 6. Average R^2 value for 1-, 2-, and 3-variable sensitivity regression for a 3-hour forecast of 80-m wind speed in the Stateline target area for all time periods and only ramp periods.

IC Variables	All Periods	Ramp Periods
One Variable		
(1) 80-m wind speed	0.168	0.180
(2) 10-m to 80-m wind shear	0.180	0.158
(3) 2-m to 80-m temperature difference	0.160	0.121
Two Variables		
(1) and (2)	0.300	0.241
(1) and (3)	0.245	0.231
(2) and (3)	0.259	0.223
Three Variables		
(1), (2) and (3)	0.300	0.282

Table 7. Average R^2 value for 1-, 2-, and 3-variable sensitivity regression for a 3-hour forecast of 80-m wind speed in the Hopkins Ridge target area for all time periods and only ramp periods.

IC Variables	All Periods	Ramp Periods
One Variable		
(1) 80-m wind speed	0.195	0.141
(2) 10-m to 80-m wind shear	0.194	0.189
(3) 2-m to 80-m temperature difference	0.149	0.229
Two Variables		
(1) and (2)	0.233	0.265
(1) and (3)	0.266	0.229
(2) and (3)	0.268	0.233
Three Variables		
(1), (2) and (3)	0.299	0.265

Table 8. Average coefficient values of the three-variable sensitivity regression for a 3-hour forecast of 80-m wind speed in the Klondike target area for all time periods and only ramp periods.

IC Variables	All Periods	Ramp Periods
Three Variables		
(1) 80-m wind speed	0.260	0.095
(2) 10-m to 80-m wind shear	0.251	0.284
(3) 2-m to 80-m temperature difference	0.037	0.213

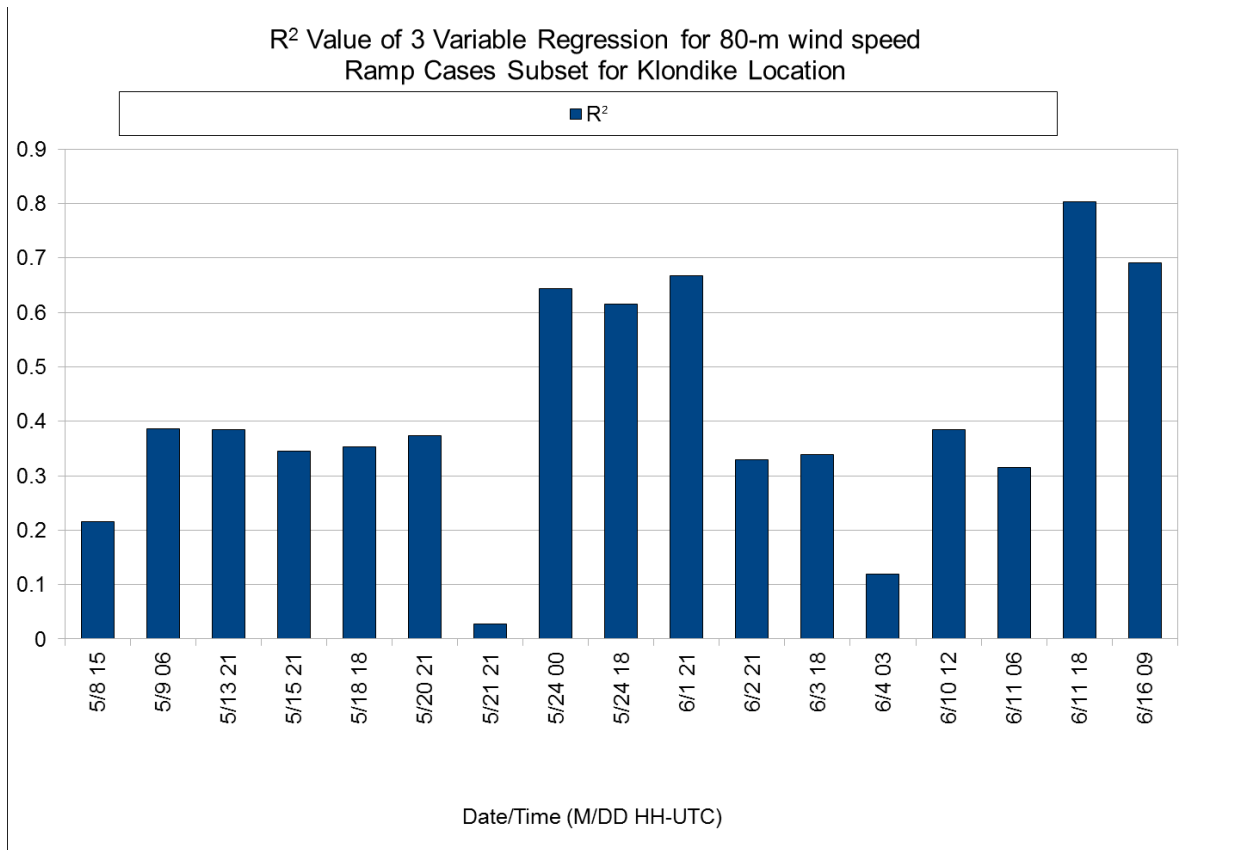


Figure 21. R² value for a multiple regression of three normalized IC variables from their respective points of maximum average 47-day sensitivity for a 3-hour forecast of the average 80-m wind speed in the Klondike metric box for each of 17 ramp events.

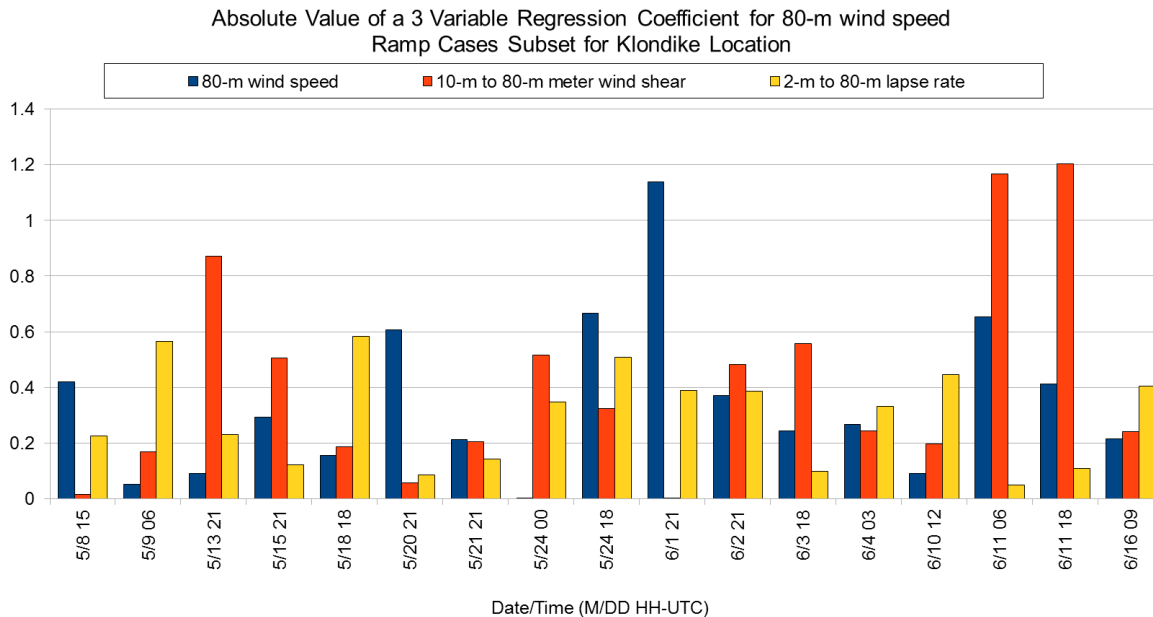


Figure 22. Absolute value of the regression coefficient for combinations of three normalized IC variables from their respective points of maximum average ramp case R^2 value for 3-hour forecasts of 80-m wind speed in the Klondike metric box for each of 17 ramp events.

The MOOA analysis suggests that it is necessary to utilize all three of the identified variables/locations in order to achieve consistent value for the ramp event cases. However, there is likely more information to be extracted from the sensitivity dataset given that several factors were not considered in this preliminary analysis.

One issue is that the locations of the second and third variables were chosen based on the maximum single variable regression R^2 value. However, the locations of maximum R^2 for each variable are not necessarily the locations that will achieve the highest R^2 for a 2- or 3-variable regression. It is certainly possible that the maximum R^2 locations may be more strongly correlated with each other than other sites with somewhat lower R^2 . In this case, it is conceivable that a combination of two or three sites, several with R^2 values less than the maximum for single variable regression, will produce the highest R^2 value for multivariable regression.

One method to test a larger set of variables and locations would be to start with the location of highest R^2 for a single variable. A two-variable regression could be performed with this point and every grid point for the second variable. A map of the 2-variable regression R^2 values could be created. Then the location would be selected that produces the maximum 2-variable R^2 . A 3-variable regression would be done for these two variables and locations as well as every grid point location of the third variable. A second R^2 map would be extracted. Finally, the location that produced the maximum 3-variable regression R^2 would be selected. Although this exercise would be computationally intensive, it would help to determine the optimal location for additional observations given a known first location and variable.

5. Summary

In past research, the ensemble sensitivity analysis (ESA) has been applied to large-scale weather prediction. Zack et al. (2010) extended the ESA method to the mesoscale by adding a multiple observation optimization algorithm (MOOA) to analyze forecast sensitivity in the Tehachapi Pass region of California. The ESA-MOOA approach was used in the current effort to study forecast sensitivities of 80-m wind speed in the Washington-Oregon region.

The ESA-MOOA is based on statistical analysis of data from an ensemble of NWP model simulations for an analysis period that is representative of the weather regimes in the area of interest. The ensemble members differ from each other due to perturbations introduced in the initial and boundary conditions of the simulations. The resulting analyses are used to estimate forecast sensitivity to prior values of atmospheric state variables for selected variables and look-ahead periods. One or more composites (e.g. averages, frequency) of forecast sensitivity parameters can then be generated to provide information about the climatological sensitivity patterns. These composite patterns can, in turn, provide guidance on where to deploy meteorological sensors to achieve the greatest impact on forecast performance for the desired variable and look-ahead period.

The ESA-MOOA was applied to the Mid-Columbia Basin using the WRF 2.2 atmospheric model and DART data assimilation software. An ensemble of 48 members was generated over a period extending from 1 May to 19 June 2007. The first two days were considered to be a spin-up period for the ensemble and were excluded from the forecast sensitivity calculations. Output was saved every hour and the forecast sensitivity for 1- to 3-hour look-ahead periods was computed from the hourly output data. Twelve prior state variables were considered in the analysis. Three areas of interest were examined along the Mid-Columbia Basin at Hopkins Ridge, Stateline, and Klondike. The forecast sensitivity was computed for all time periods in the sample as well as a ramp event subsample for all three sites of interest. The ramp event subsample consisted of 17 to 19 time periods for each site in which large changes (up or down) in wind power production occurred in a 3-hour or shorter period.

The forecast sensitivities showed that some initial conditions (IC) variables had a low impact on the forecast. Other initial states produced very localized and high sensitivity areas in which the 80-m wind speed forecast at one of the target locations was highly correlated to the IC variables. This result was quite different from the Tehachapi Pass study (Zack et al. 2010) which found well-defined, localized patterns of high sensitivity for a number of prior state variables. The differences in sensitivity intensity and patterns between Tehachapi Pass and the Mid-Columbia Basin are consistent with the physical processes that drive the wind patterns in both areas. The primarily warm season, diurnal cycles that dominate the weather in Tehachapi Pass result in well-defined sensitivity patterns, while the Mid-Columbia Basin region is affected by larger scale flow regimes resulting in less defined and weaker sensitivity patterns.

The most consistently sensitive variables for the Mid-Columbia Basin forecast targets were: (1) 80-m wind speed, (2) 10-m to 80-m wind shear, and (3) 2-m to 80-m vertical temperature

gradient. These variables showed regions of high sensitivity and explained variance extending from the Columbia Gorge along and just south of the Mid-Columbia Basin stretching into far eastern Washington State. Areas within the Mid-Columbia Basin showed correlations to all three sites. This result suggests that a relatively small number of observations in this area would have a beneficial impact on the 80-m wind speed forecast at all three target locations.

The MOOA was applied using the locations with highest explained variance (R^2) of the average sensitivity over the complete 47-day period and also a subsample of the 20 ramp events. The high-sensitivity locations were mainly to the west of the target locations. The only exception was the area of sensitivity to low-level temperature gradient, which is located in regions of high terrain well removed from the target region.

Results from the MOOA suggest that the greatest benefit would come from observing all three variables examined, as shown by high values of explained variance (R^2). When broken down to single variable correlations, the 80-m wind speed and 10-m to 80-m wind shear produced equally high R^2 values, indicating the importance of each single observation. This result applied for both the full 47-day period and the ramp event subsample at all three locations. Although these two variables produced strong R^2 values, 2-m to 80-m temperature gradients are also correlated with 80-m wind speed three hours ahead at Klondike, especially for ramp cases. Therefore, all variables should be considered when adding future observations, since each one contributes information to the model initial state.

The results demonstrate that the methods used in this study can produce physically consistent forecast sensitivity, explained variance, and statistically significant frequency results on mesoscale space and time scales. In addition, they can be used to provide specific and physically reasonable guidance for the design of sensor networks intended to improve forecast performance of specific variables at target locations.

There are number of possibilities for extending the pioneering work done in this study. Forecast sensitivity and other computed fields as well as observation deployment strategies derived from them were not validated. Such validation is essential before using the methodology as a routine tool to formulate sensor network deployment strategies. These issues could be addressed by observation denial experiments using actual data gathered at target locations or observing system simulation experiments (OSSEs; Kalnay et al. 1985; Arnold and Dey 1986).

Data denial and/or OSSEs would reveal whether the highly sensitive areas do indeed have a significant impact on the prediction of 80-m wind speed at target locations. The analysis could be stratified by events or weather regimes to determine the value of observations for critical events. Regime-based analysis could help determine where observations might be needed in regions that are sensitive to highly variable flows instead of focusing on the most common patterns. Also, performing experiments over a longer time period could help account for biases related to season and current weather regime as well as address issues of representativeness given the limited sample size.

The analysis could also be expanded to include other prior state variables such as time-varying or spatially-varying fields in addition to the twelve considered in this study. Finally, the MOOA could be enhanced to consider multiple locations from each prior state variable, using locations from multivariate regressions, in addition to the maximum average explained variance (R^2) of a univariate regression considered here. Other possibilities include using the field of highest significant sensitivity frequency to determine the location for multivariate regression. When trying to find one observation location that can benefit multiple target locations, a cost function approach combining sensitivity magnitude and R^2 values (or significant sensitivity) for multiple target locations could prove useful.

6. Acknowledgements

This work performed under the auspices of the U.S. Department of Energy by Lawrence Livermore National Laboratory under Contract DE-AC52-07NA27344. The work of the authors from AWS Truepower was performed under subcontract B584259 from Lawrence Livermore National Laboratory.

7. Reference

- Ancell, B. and G. J. Hakim, 2007: Comparing adjoint- and ensemble-sensitivity analysis with applications to observation targeting. *Mon. Wea. Rev.*, **135**, 4117-4134.
- Anderson, J. L., 2001: An ensemble adjustment Kalman filter for data assimilation. *Mon. Wea. Rev.*, **129**, 2884-2903.
- Anderson, J. L., 2007: An adaptive covariance inflation error correction algorithm for ensemble filters. *Tellus*, 59A, 210-224.
- Anderson, J. L., and S. L. Anderson, 1999: A Monte Carlo implementation of the nonlinear filtering problem to produce ensemble assimilations and forecasts. *Mon. Wea. Rev.* 127, 2741-2758.
- Anderson, J. L., T. Hoar, K. Raeder, H. Liu, N. Collins, R. Torn, and A. F. Arellano, 2009: The Data Assimilation Research Testbed: A community data assimilation facility. *Bull. Amer. Meteor. Soc.*, **90**, 1283-1296.
- Arnold, C. P. Jr., and C. H. Dey, 1986: Observing-system simulation experiments: Past, present, and future. *Bull. Amer. Meteor. Soc.*, **67**, pp. 687-695.
- Evensen, G., 2007: Data assimilation: The ensemble Kalman filter, Springer, Berlin, 307 pp.

- Houtekamer P. and H. L. Mitchell, 1998: Data assimilation using an ensemble Kalman filter technique, *Mon. Wea. Rev.*, **126**, 796-811.
- Kalnay, E., R. Atlas, and M. Halem, 1985: The impact of satellite temperature sounding and wind data on numerical weather prediction. *Optical Engineering*, **24**, 341-346.
- Skamarock, W. C., J. B. Klemp, J. Dudhia, D. O. Gill, D. M. Barker, W. Wang, and J. G. Powers, 2005: A Description of the Advanced Research WRF Version 2, NCAR TECHNICAL NOTE: NCAR/TN-468+STR, National Center for Atmospheric Research, Boulder, Colorado, USA.
- Torn, R. D., and G. J. Hakim, 2008: Ensemble-based sensitivity analysis. *Mon. Wea. Rev.*, **136**, 663-677.
- Zack, J., E. Natenberg, S. Young, J. Manobianco, and C. Kamath, 2010: Application of ensemble sensitivity analysis to observation targeting for short-term wind speed forecasting. Technical Report LLNL-TR-424442, 32 pp., Lawrence Livermore National Laboratory, Livermore, CA.

Appendix A: Specifications of the ESA Configuration

Table A-1. Configuration of the WRF 2.2 model and grid used in this investigation

Grid

- Matrix Size (NX,NY,NZ): Outer Grid: 120 X 120 X 38, Inner Grid: 172 X160 X 38
- Grid cell size: Outer Grid ~12 km, Inner Grid ~ 4 km

Model Configuration

- WRF single-moment (WSM) 3-class ice scheme
- Long wave radiation scheme: Rapid radiative transfer model
- Short wave radiation scheme: Dudhia scheme
- Boundary layer scheme: YSU scheme
- No convective parameterization
- 60 second time step on outer grid, 20-second time step on inner grid
- Runge-Kutta 3rd order time integration
- Horizontal Smagorinsky 1st order closure
- 6th-order numerical diffusion turned on

Table A-2. Configuration of the Data Assimilation Research Testbed (DART) module

- Square root Ensemble Kalman Filter
- Cycled every 6 hours 4 times a day with various observations
- Ensemble size: 48 members
- Perturbed IC from National Weather Service (NWS) Rapid Update Cycle (RUC) for first cycle
- Perturbed boundary conditions for each assimilation period, boundary conditions also from RUC
- Deterministic inflation based on spatially-varying state space (I.e. covariance inflation)
- Initial inflation standard deviation 0.6
- Initial inflation 1.0

Table A-3. Data Assimilated Every 6 Hours into the Ensemble of Simulations

Assimilated Observations

'RADIOSONDE_TEMPERATURE',
'RADIOSONDE_U_WIND_COMPONENT',
'RADIOSONDE_V_WIND_COMPONENT',
'RADIOSONDE_SPECIFIC_HUMIDITY',
'ACARS_TEMPERATURE',
'ACARS_U_WIND_COMPONENT',
'ACARS_V_WIND_COMPONENT',
'ACARS_SPECIFIC_HUMIDITY',
'MARINE_SFC_TEMPERATURE',
'MARINE_SFC_SPECIFIC_HUMIDITY',
'RADIOSONDE_SURFACE_ALTIMETER',
'MARINE_SFC_ALTIMETER',
'LAND_SFC_ALTIMETER',

Evaluated observations

'METAR_TEMPERATURE_2_METER',
'METAR_U_10_METER_WIND',
'METAR_V_10_METER_WIND',
'MARINE_SFC_U_WIND_COMPONENT',
'MARINE_SFC_V_WIND_COMPONENT',
'LAND_SFC_U_WIND_COMPONENT',
'LAND_SFC_V_WIND_COMPONENT',
'DEW_POINT_2_METER',/
'LAND_SFC_TEMPERATURE',
'LAND_SFC_SPECIFIC_HUMIDITY',

Appendix B: Table of Ramp Events

Table B1. List of large ramp events used to define the ramp subsample for the sensitivity analysis for Hopkins Ridge.

Start Time (YYYY MMDD HHmm) (UTC)	Amplitude (% Capacity) 156.6 MW	Maximum 5- minute ramp rate (% Capacity)	Duration (minutes)
Upward Ramps			
2007 0604 2110	98.7	20.3	120.0
2007 0523 2310	98.0	57.2	120.0
2007 0521 2250	96.9	17.5	110.0
2007 0603 1940	95.7	66.4	100.0
2007 0518 2040	95.4	39.0	120.0
2007 0512 1610	94.0	26.6	120.0
2007 0604 1640	93.6	31.4	90.0
2007 0520 2220	87.9	20.8	110.0
2007 0526 2330	92.3	33.8	130.0
2007 0604 0050	86.4	27.2	120.0
Downward Ramps			
2007 0604 1810	-98.8	-30.8	90.0
2007 0603 2120	-97.1	-19.4	110.0
2007 0521 2020	-90.6	-22.0	110.0
2007 0614 0850	-80.5	-11.9	130.0
2007 0605 0040	-77.5	-20.7	120.0
2007 0511 0210	-72.9	-14.6	100.0
2007 0528 1050	-72.4	-13.9	120.0
2007 0521 1410	-73.2	-9.8	130.0
2007 0508 1450	-74.3	-12.5	130.0
2007 0517 0240	-70.1	-17.6	120.0

Table B2. List of large ramp events used to define the ramp subsample for the sensitivity analysis for Stateline.

Start Time (YYYY MMDD HHmm) (UTC)	Amplitude (% Capacity) 300 MW	Maximum 10- minute ramp rate (% Capacity)	Duration (minutes)
Upward Ramps			
2007 0512 1510	91.1	28.8	120.0
2007 0603 1950	91.0	64.2	70.0
2007 0604 2050	87.2	32.2	110.0
2007 0603 2210	81.2	23.0	110.0
2007 0523 2150	79.6	21.7	120.0
2007 0518 2000	78.6	17.2	120.0
2007 0521 1710	75.6	21.0	110.0
2007 0510 2140	86.3	11.7	170.0
2007 0606 2140	73.9	14.4	120.0
2007 0508 1800	77.0	18.5	130.0
Downward Ramps			
2007 0604 2350	-89.7	-17.5	120.0
2007 0603 2100	-88.0	-34.0	70.0
2007 0606 1730	-83.7	-15.0	160.0
2007 0521 1910	-68.6	-18.9	120.0
2007 0602 0010	-62.5	-13.5	120.0
2007 0506 0930	-61.6	-6.6	130.0
2007 0524 0150	-57.3	-16.4	100.0
2007 0513 1130	-61.6	-8.4	150.0
2007 0528 1000	-76.4	-6.4	220.0
2007 0511 0150	-50.5	-7.2	120.0

Table B3. List of large ramp events used to define the ramp subsample for the sensitivity analysis for Klondike.

Start Time (YYYY MMDD HHmm) (UTC)	Amplitude (% Capacity) 99 MW	Maximum 10- minute ramp rate (% Capacity)	Duration (minutes)
Upward Ramps			
2007 0515 2000	76.0	22.8	120.0
2007 0603 1430	75.5	26.9	120.0
2007 0508 1230	75.5	14.9	120.0
2007 0610 1020	73.9	70.3	120.0
2007 0602 1920	73.1	29.0	70.0
2007 0616 0700	72.6	61.7	120.0
2007 0601 2000	67.4	23.1	120.0
2007 0518 1430	66.8	19.5	120.0
2007 0524 1550	63.1	9.2	120.0
2007 0520 1900	63.0	27.4	120.0
Downward Ramps			
2007 0523 2020	-74.6	-61.4	110.0
2007 0513 2000	-72.7	-54.8	70.0
2007 0611 0350	-71.7	-44.3	100.0
2007 0610 0910	-69.2	-65.8	70.0
2007 0602 2050	-72.7	-20.4	130.0
2007 0611 1550	-65.4	-65.3	70.0
2007 0509 0420	-64.7	-16.8	100.0
2007 0604 0050	-62.3	-12.7	100.0
2007 0619 2210	-61.7	-15.3	120.0
2007 0603 1630	-60.7	-43.0	90.0

Appendix C: Vertical Levels of the Model

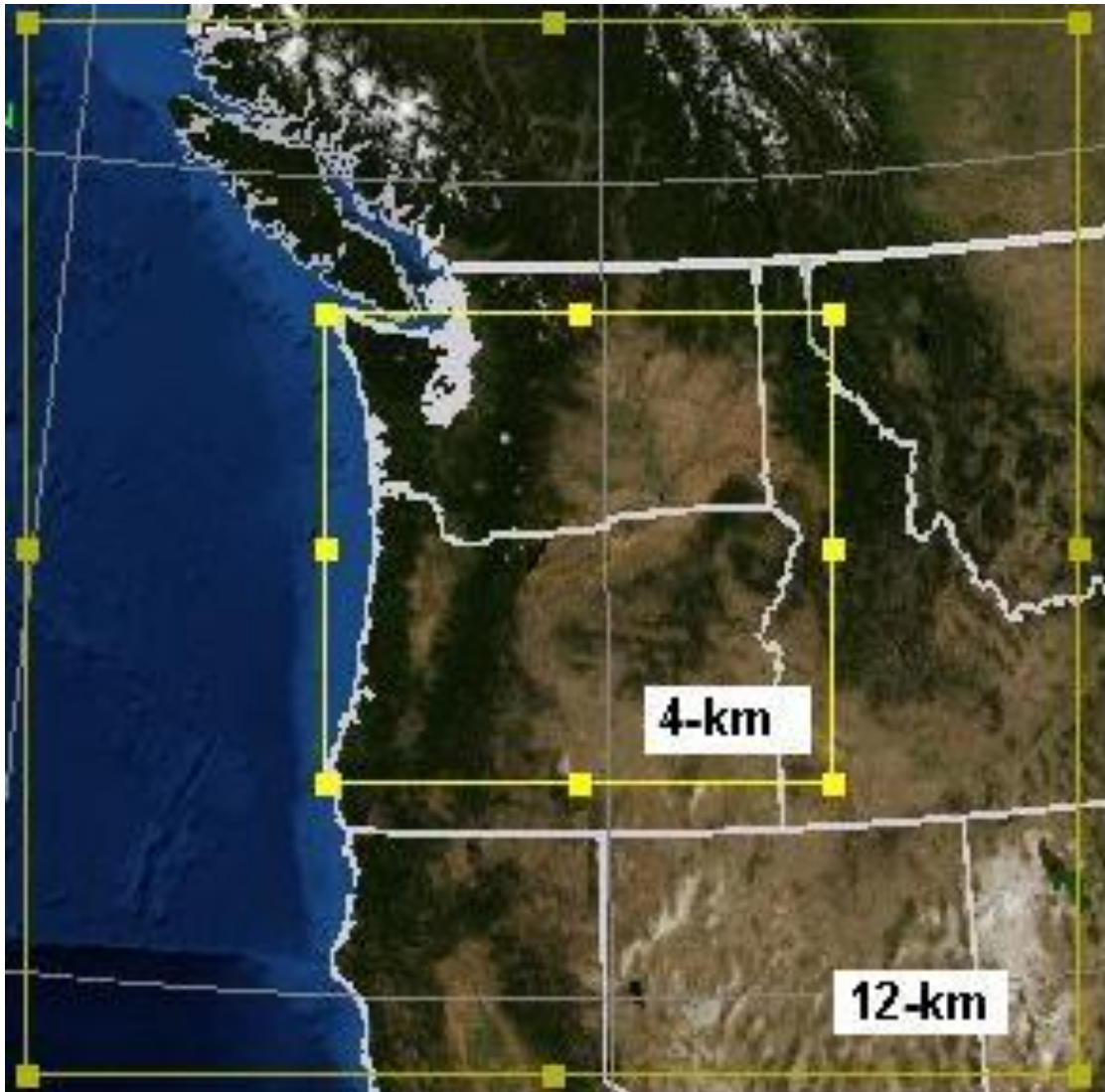


Figure C1. The figure depicts the outer (12-km) and inner (4km) nested grids. The three-dimensional nested grid matrix consisted of 120 x 120 x 40 1 points with 12-km horizontal grid spacing, and an inner grid of 172 x 160 x 40 points with 4-km spacing.

Model Level Number	Pressure Level pa	Approx. Altitude (m)	Model Level Number	Pressure Level pa	Approx. Altitude (m)
1	102444	0	21	52500	5200
2	100000	100	22	50000	5600
3	97500	300	23	47500	6000
4	95000	550	24	45000	6400
5	92500	750	25	42500	6800
6	90000	1000	26	40000	7200
7	87500	1250	27	37500	7600
8	85000	1500	28	35000	8200
9	82500	1750	29	32500	8600
10	80000	2000	30	30000	9100
11	77500	2250	31	27500	9600
12	75000	2500	32	25000	10,200
13	72500	2750	33	22500	10,900
14	70000	3000	34	20000	11,750
15	67500	3300	35	17500	12,200
16	65000	3600	36	15000	13,700
17	62500	3900	37	12500	14,700
18	60000	4200	38	10000	16,100
19	57500	4500	39	7500	20,000
20	55000	4800	40	5000	26,000

Appendix D: Additional Variable Sensitivity Results

3-km Wind Speed

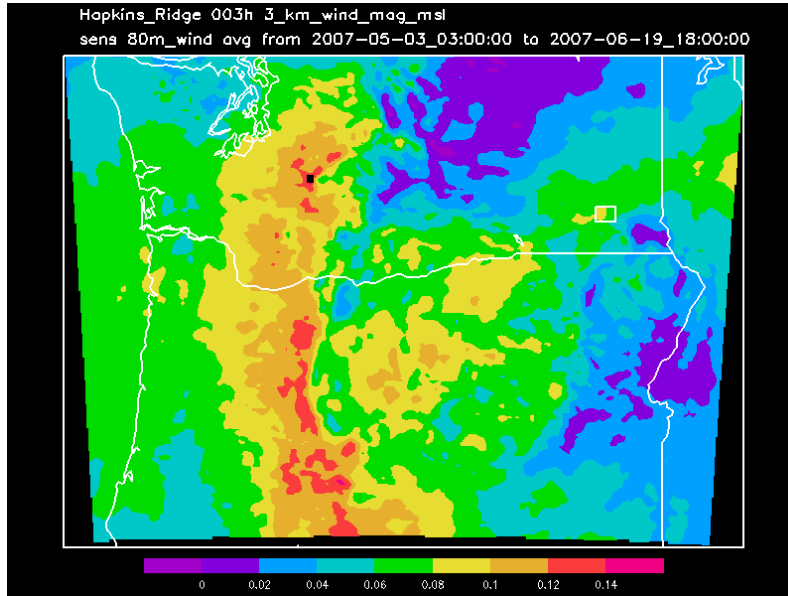


Figure D1. Average sensitivity of 80-m wind speed (m/s) within the white target box to the 3-km wind speed throughout the entire grid domain for a 3-hour ahead forecast at all time periods in the 47-day analysis period for Hopkins Ridge.

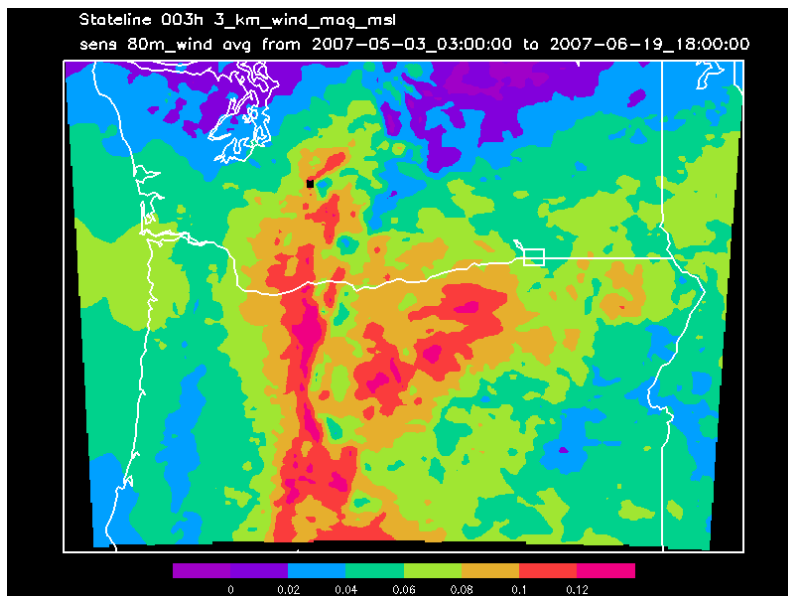


Figure D2. Average sensitivity of 80-m wind speed (m/s) within the white target box to the 3-km wind speed throughout the entire grid domain for a 3-hour ahead forecast at all time periods in the 47-day analysis period for Stateline.

10-80m Wind Shear

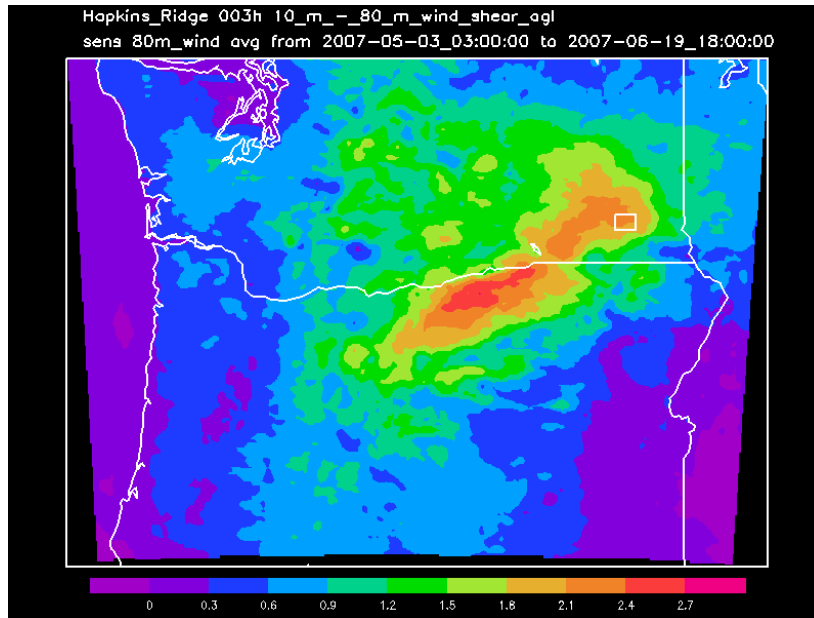


Figure D3. Average sensitivity of 80-m wind speed (m/s) within the white target box to 10-m to 80-m wind speed difference (shear) throughout the entire grid domain for a 3-hour ahead forecast at all time periods in the 47-day analysis period for Hopkins Ridge.

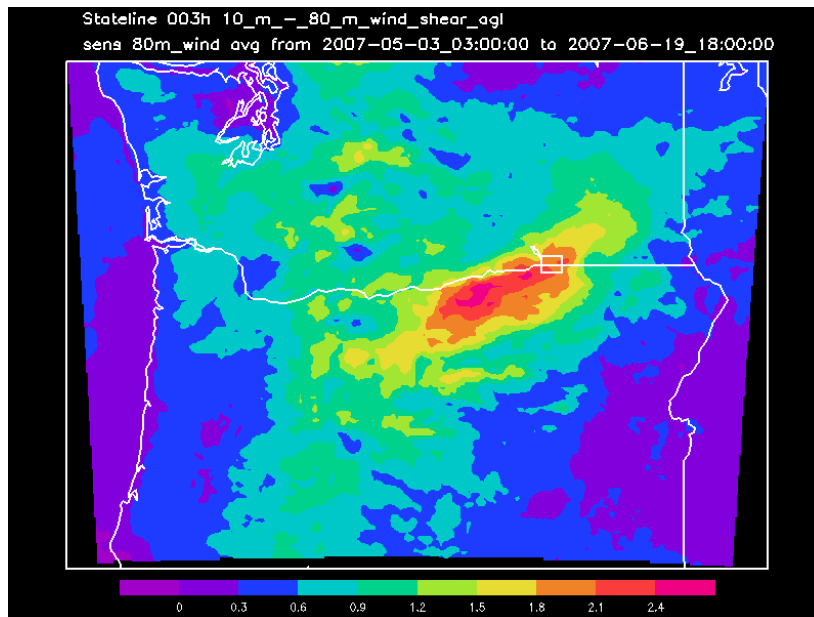


Figure D4. Average sensitivity of 80-m wind speed (m/s) within the white target box to the 10-m to 80-m wind speed difference (shear) throughout the entire grid domain for a 3-hour ahead forecast at all time periods in the 47-day analysis period for Stateline.

2-m Temperature

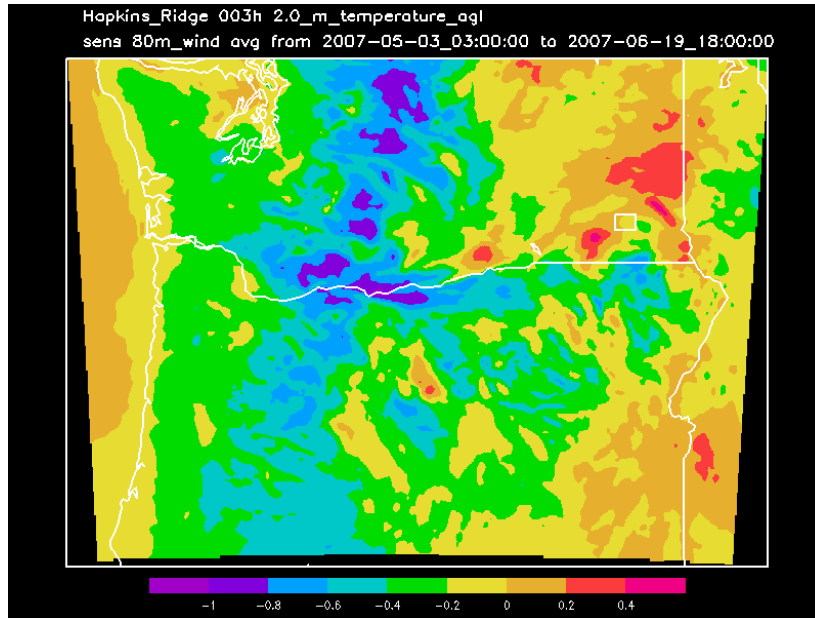


Figure D5. Average sensitivity of 80-m wind speed (m/s) within the white target box to the 2-m temperature throughout the entire grid domain for a 3-hour ahead forecast at all time periods in the 47-day analysis period for Hopkins Ridge.

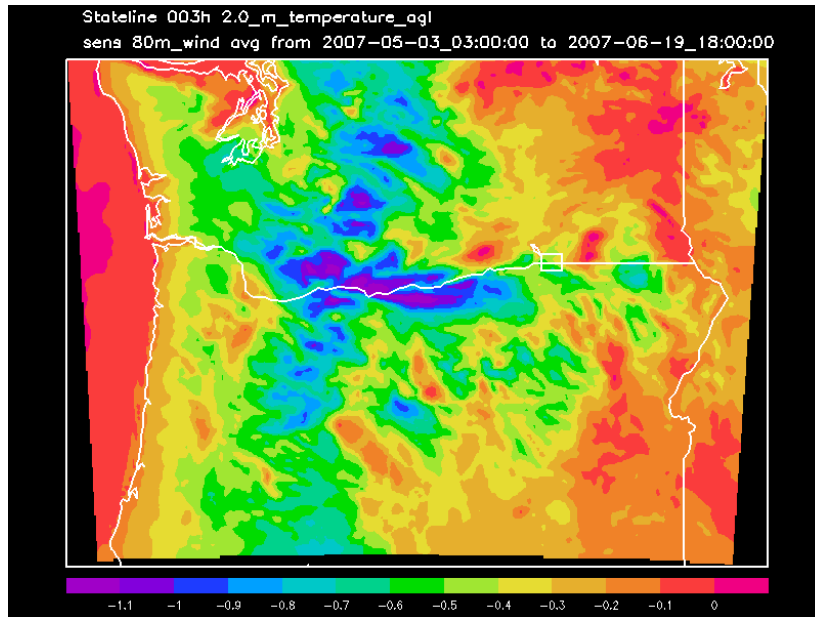


Figure D6. Average sensitivity of 80-m wind speed (m/s) within the white target box to the 2-m temperature difference throughout the entire grid domain for a 3-hour ahead forecast at all time periods in the 47-day analysis period for Stateline.

2-m to 80-m Temperature Lapse Rate

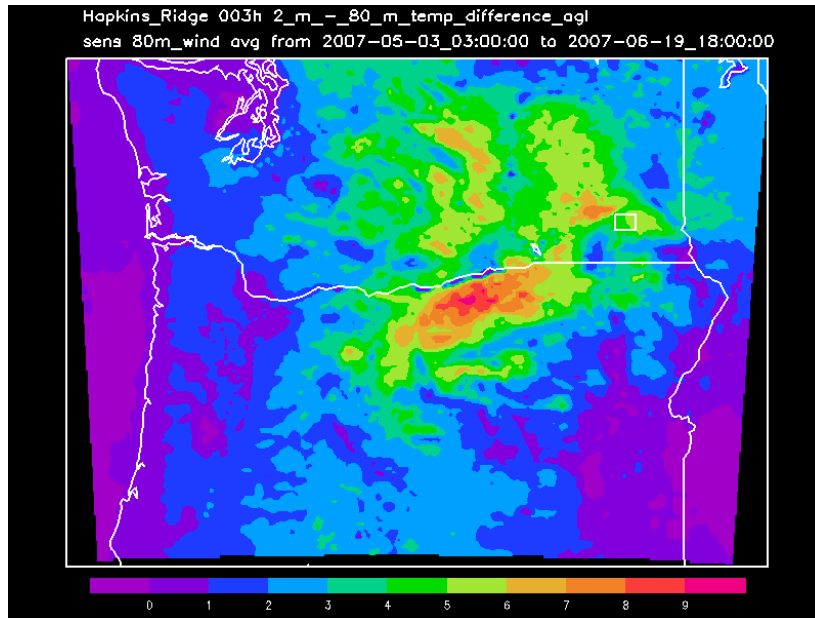


Figure D7. Average sensitivity of 80-m wind speed (m/s) within the white target box to 2-m to 80-m temperature difference (lapse rate) throughout the entire grid domain for a 3-hour ahead forecast at all time periods in the 47-day analysis period for Hopkins Ridge

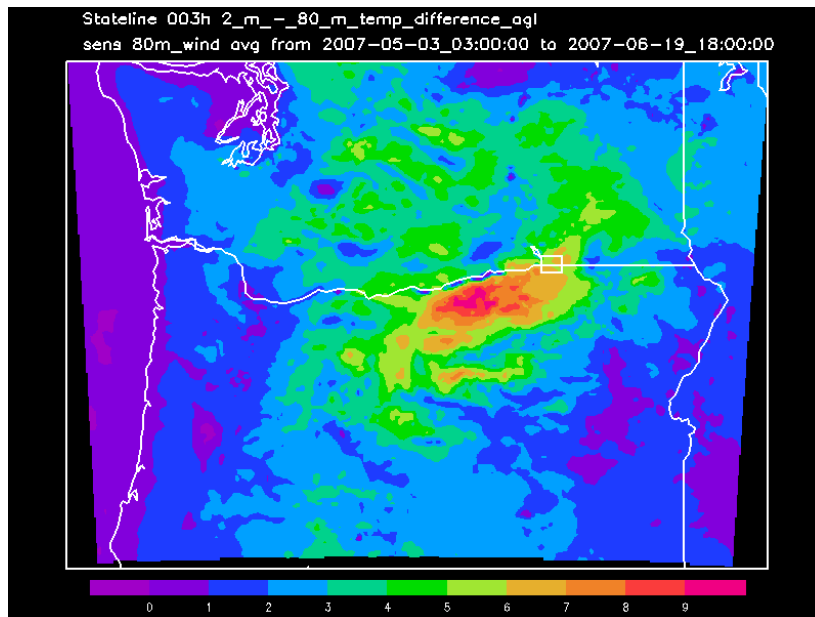


Figure D8. Average sensitivity of 80-m wind speed (m/s) within the white target box to 2-m to 80-m temperature difference (lapse rate) throughout the entire grid domain for a 3-hour ahead forecast at all time periods in the 47-day analysis period for Stateline.

Appendix E: Additional Sensitivity Results for Klondike for Stateline and Hopkins's Ridge

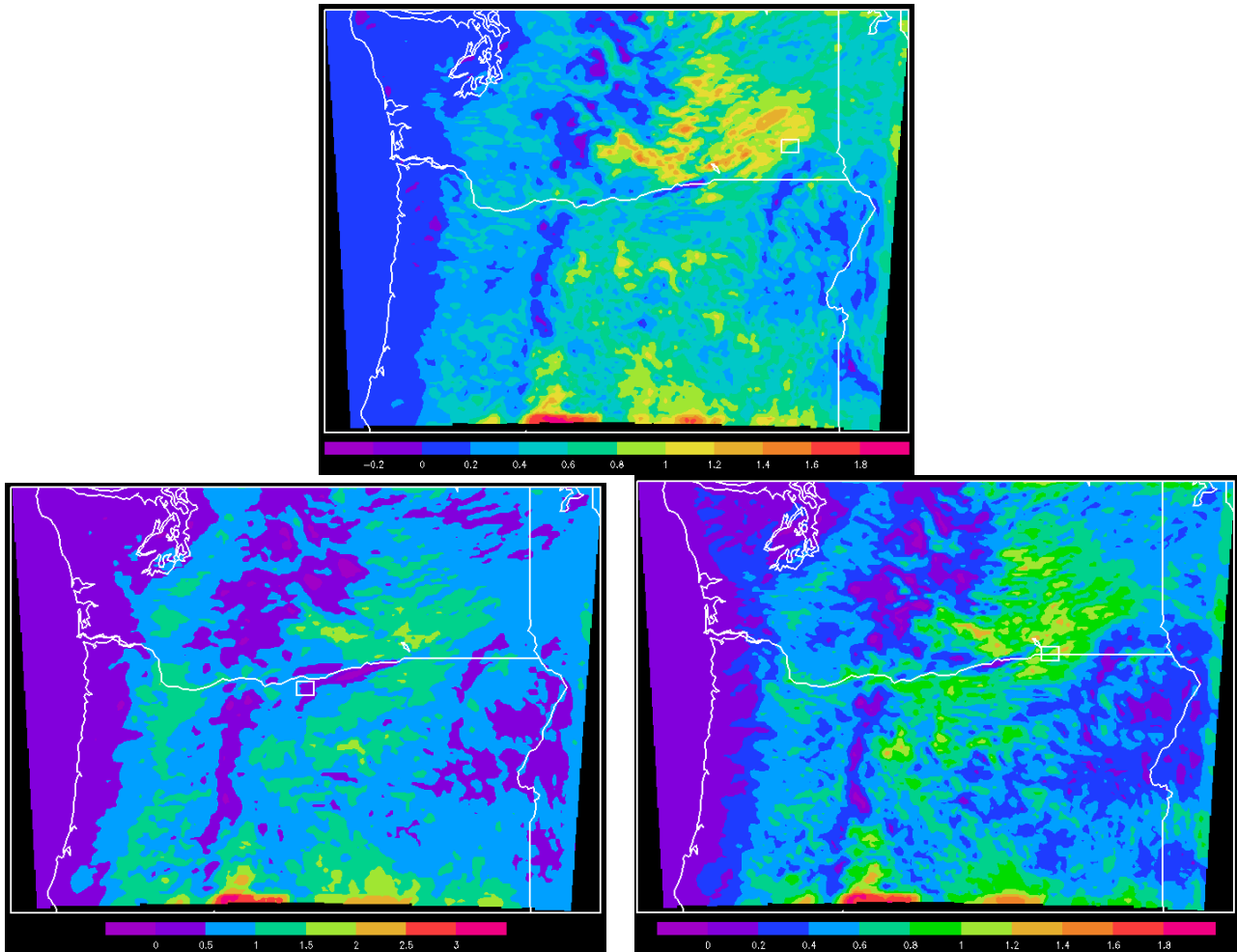


Figure E1. Average sensitivity of 80-m wind speed (m/s) within the white target box to 80-m to 1-km temperature difference throughout the entire grid domain for a 3-hour ahead forecast at all time periods in the 47-day analysis period for Hopkins Ridge (top), Klondike (bottom left), and Stateline (bottom right).

Appendix F: R² Plots

1-Hour Ahead Hopkins Ridge

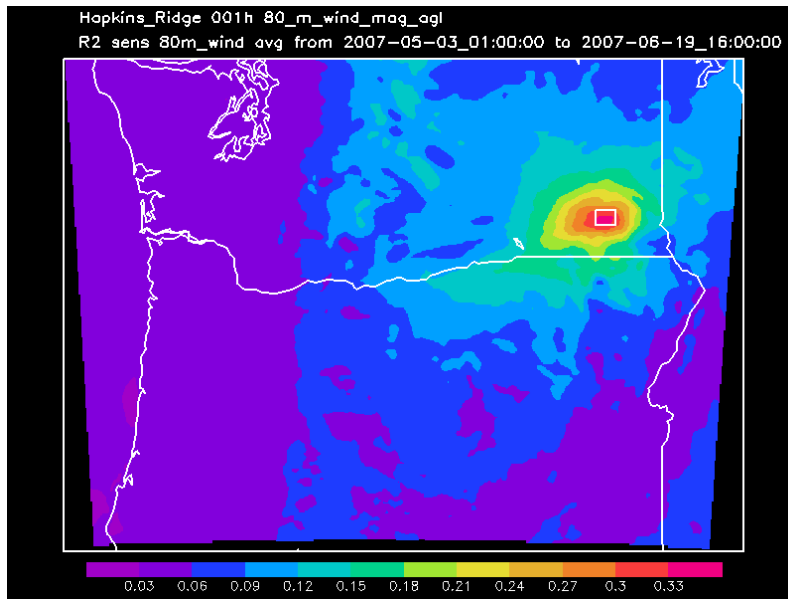


Figure F1. Average R² of 80-m wind speed (m/s) within the white target box to the 80-m wind speed throughout the entire grid domain for a 1-hour ahead forecast at all time periods in the 47-day analysis period for Hopkins Ridge.

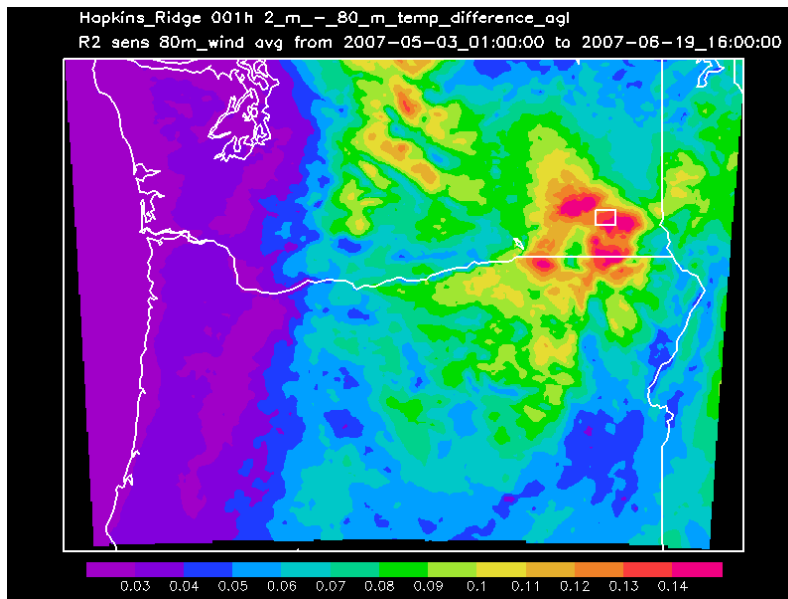


Figure F2. Average R² of 80-m wind speed (m/s) within the white target box to 2-m to 80-m temperature difference for a 1-hour ahead forecast at all times in the analysis period for Hopkins Ridge.

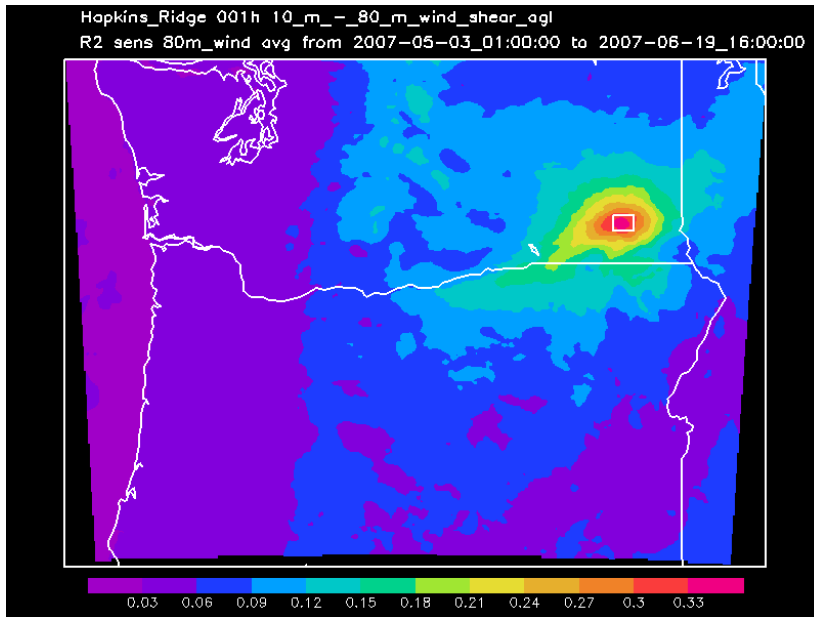


Figure F3. Average R^2 sensitivity 80-m wind speed (m/s) within the white target box to 10-m to 80-m wind speed difference for a 1-hour ahead forecast at all times in the analysis period for Hopkins Ridge.

1-Hour Ahead Stateline

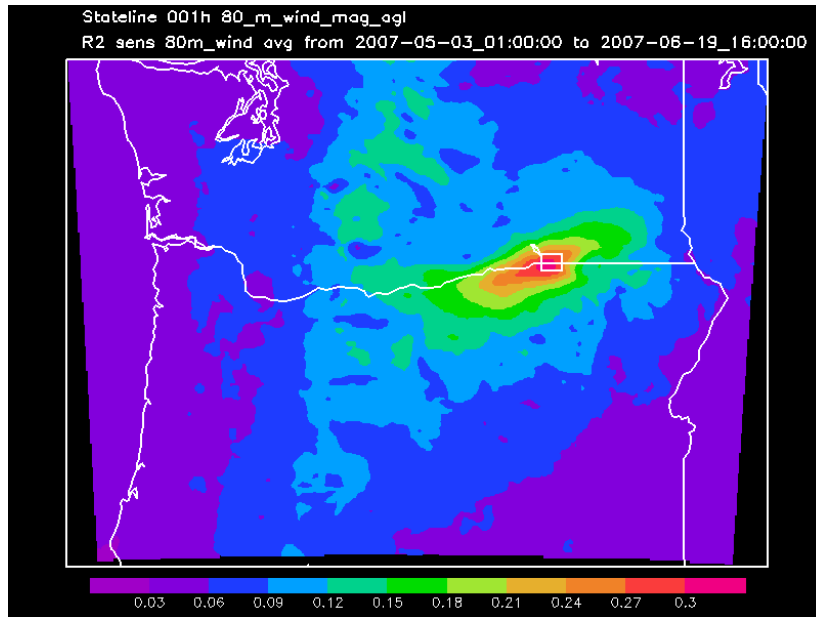


Figure F4. Average R^2 of 80-m wind speed (m/s) within the white target box to the 80-m wind speed throughout the entire grid domain for a 1-hour ahead forecast at all time periods in the 47-day analysis period for Stateline.

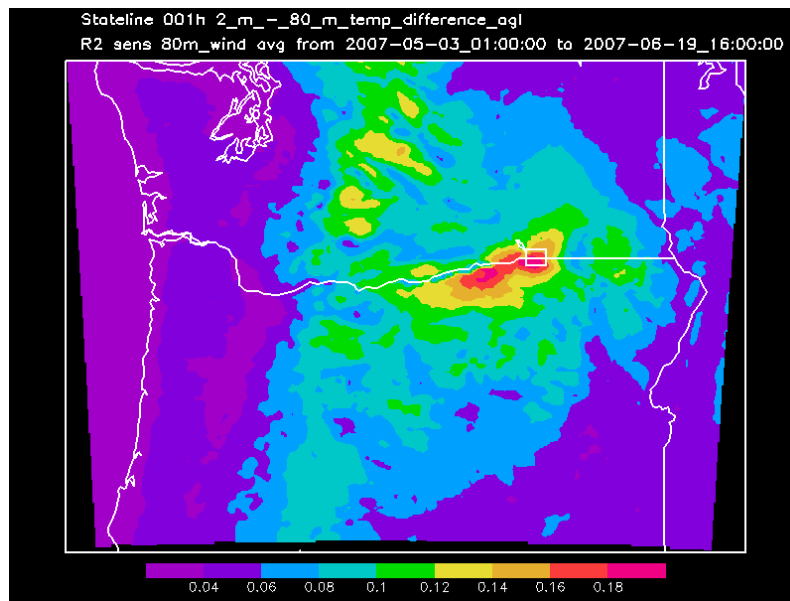


Figure F5. Average R^2 of 80-m wind speed (m/s) within the white target box to 2-m to 80-m temperature difference throughout the entire grid domain for a 1-hour ahead forecast at all times in the 47-day analysis period for Stateline.

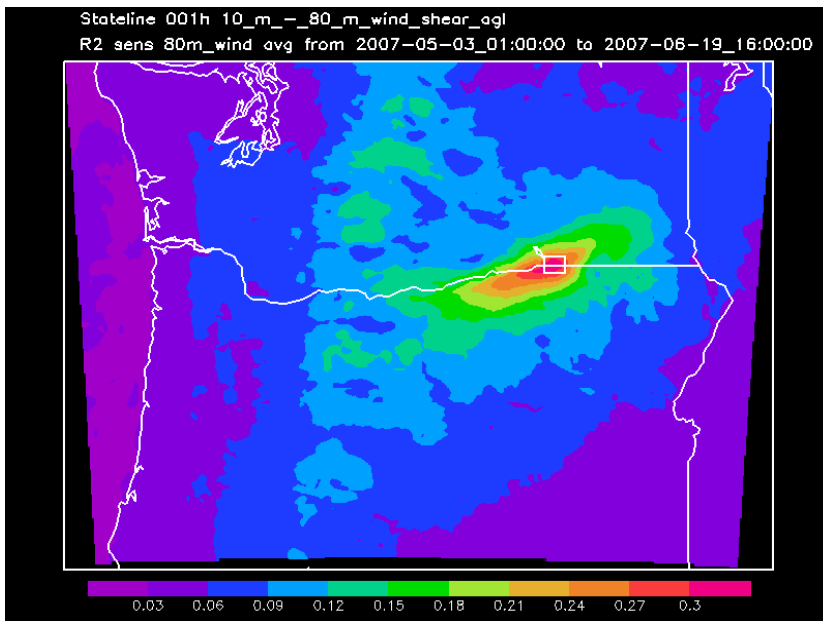


Figure F6. Average R^2 of 80-m wind speed (m/s) within the white target box to 10-m to 80-m wind speed difference throughout the entire grid domain for a 1-hour ahead forecast at all times in the analysis period for Stateline.

1-Hour Ahead Klondike

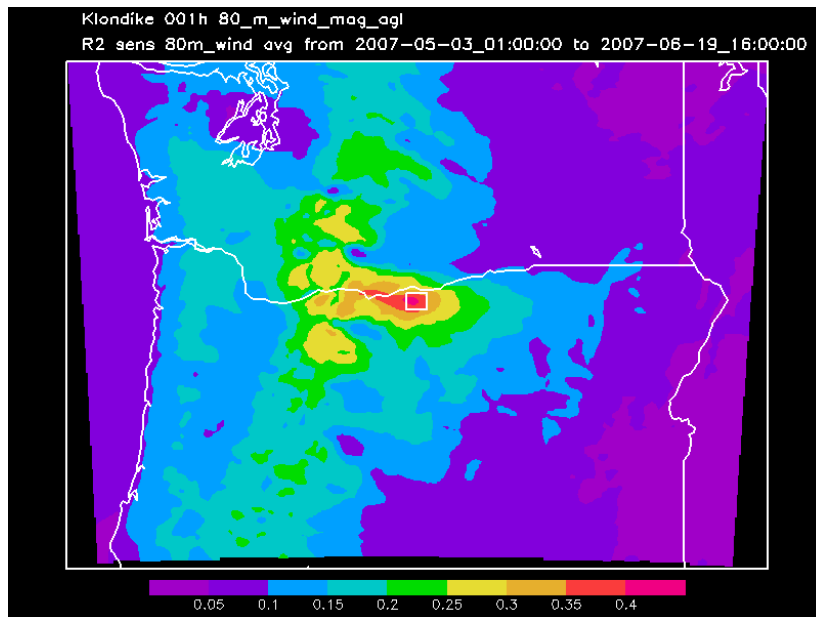


Figure F7. Average R^2 of 80-m wind speed (m/s) within the white target box to the 80-m wind speed throughout the entire grid domain for a 1-hour ahead forecast at all time periods in the 47-day analysis period for Klondike.

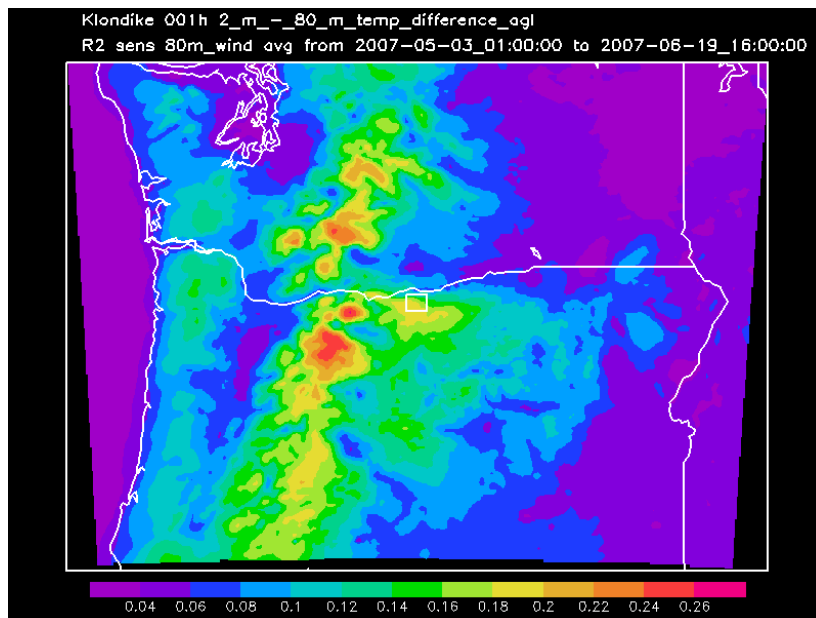


Figure F8. Average R^2 of 80-m wind speed (m/s) within the white target box to 2-m to 80-m temperature difference throughout the entire grid domain for a 1-hour ahead forecast at all times in the analysis period for Klondike.

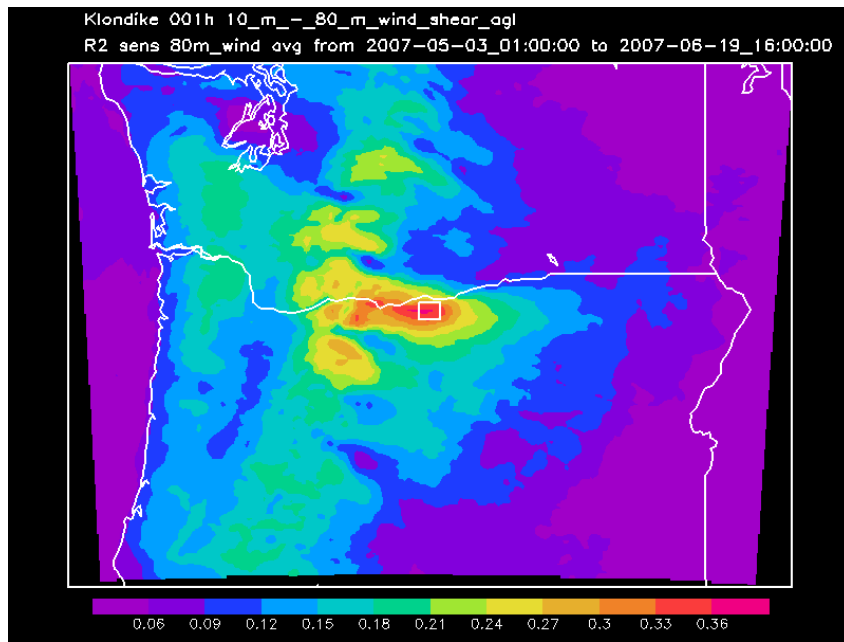


Figure F9. Average R^2 of 80-m wind speed (m/s) within the white target box to 10-m to 80-m wind speed difference throughout the entire grid domain for a 1-hour ahead forecast at all times in the analysis period for Klondike.

3-Hour Ahead Hopkins Ridge

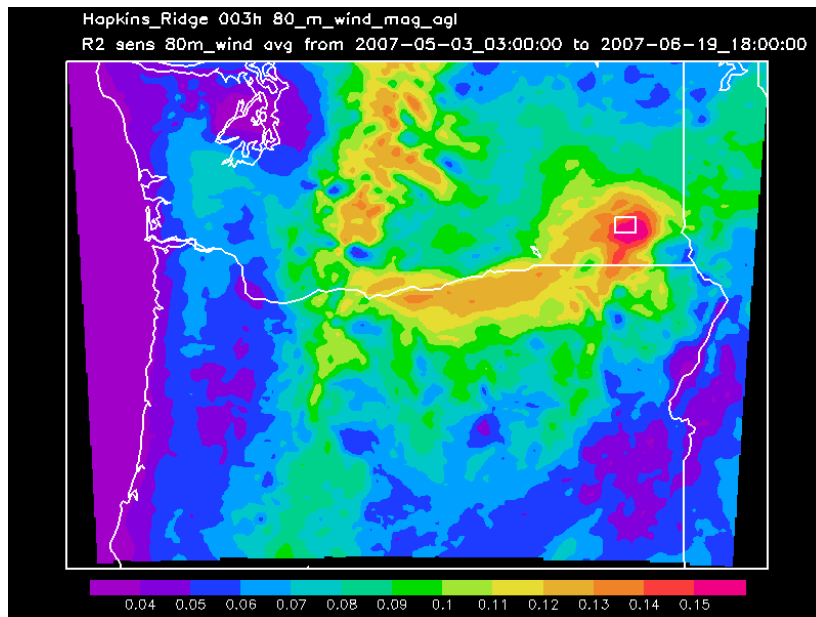


Figure F10. Average R^2 of 80-m wind speed (m/s) within the white target box to the 80-m wind speed throughout the entire grid domain for a 3-hour ahead forecast at all time periods in the 47-day analysis period for Hopkins Ridge.

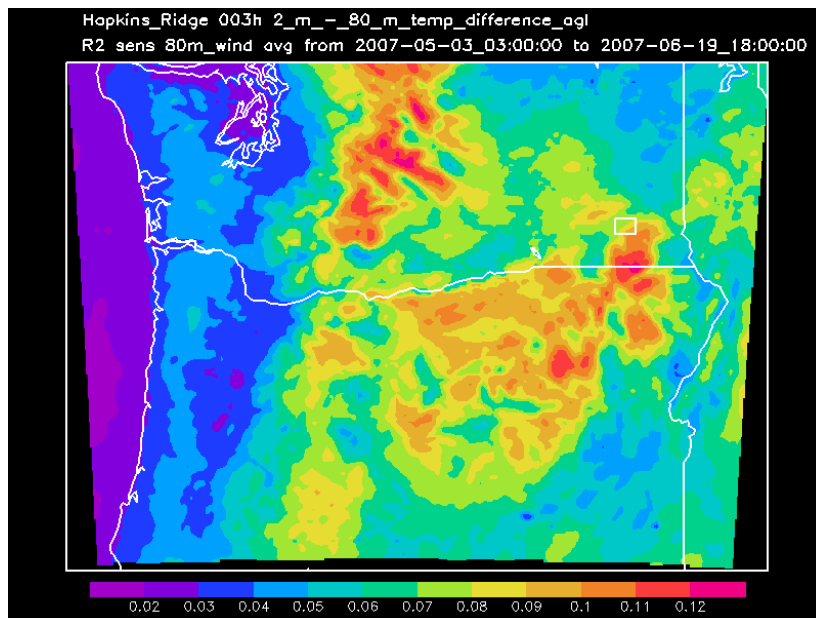


Figure F11. Average R^2 of 80-m wind speed (m/s) within the white target box to 2-m to 80-m temperature difference throughout the entire grid domain for a 3-hour ahead forecast at all times in the analysis period for Hopkins Ridge.

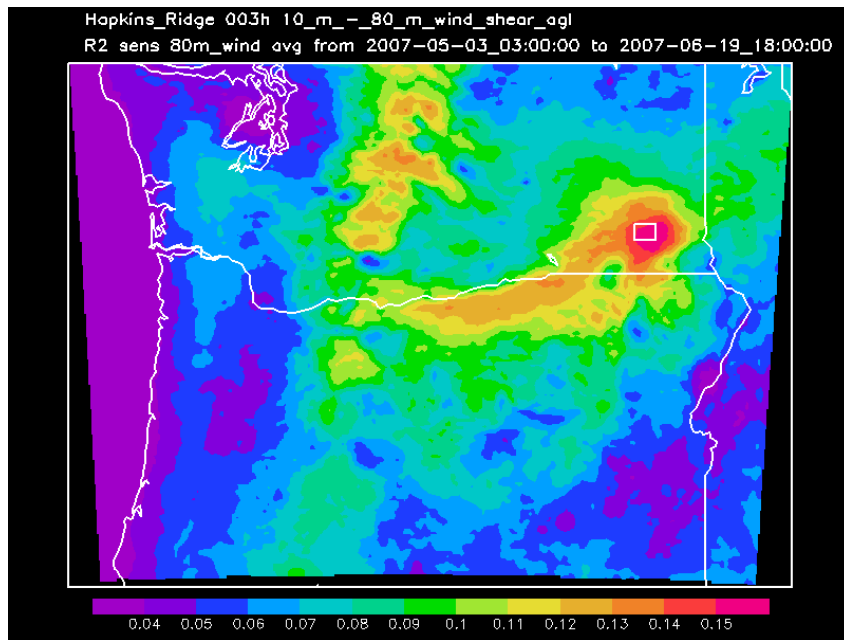


Figure F12. Average R^2 of 80-m wind speed (m/s) within the white target box to 10-m to 80-m wind speed difference throughout the entire grid domain for a 3-hour ahead forecast at all times in the analysis period for Hopkins Ridge.

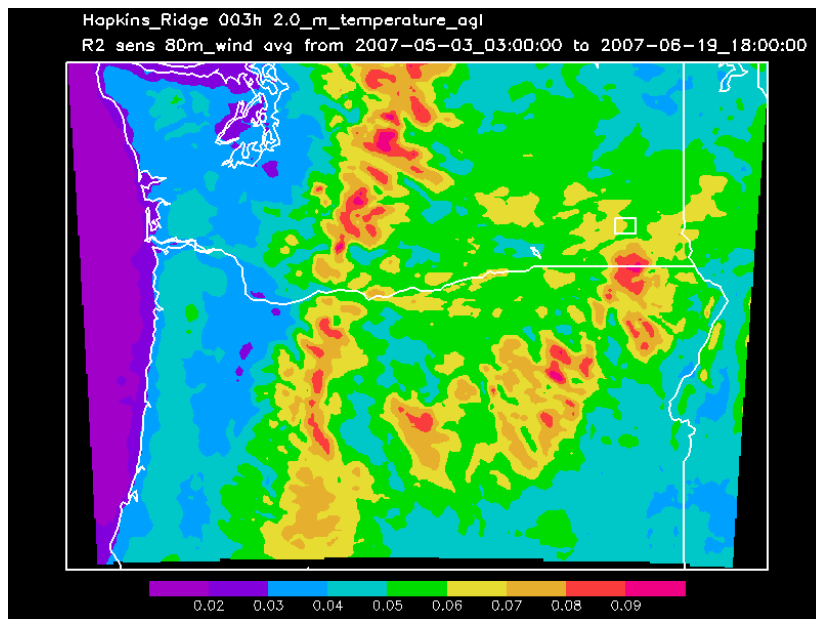


Figure F13. Average R^2 of 80-m wind speed (m/s) within the white target box to 2-m temperature throughout the entire grid domain for a 3-hour ahead forecast for all times in the analysis period for Hopkins Ridge.

3-Hour Ahead Stateline

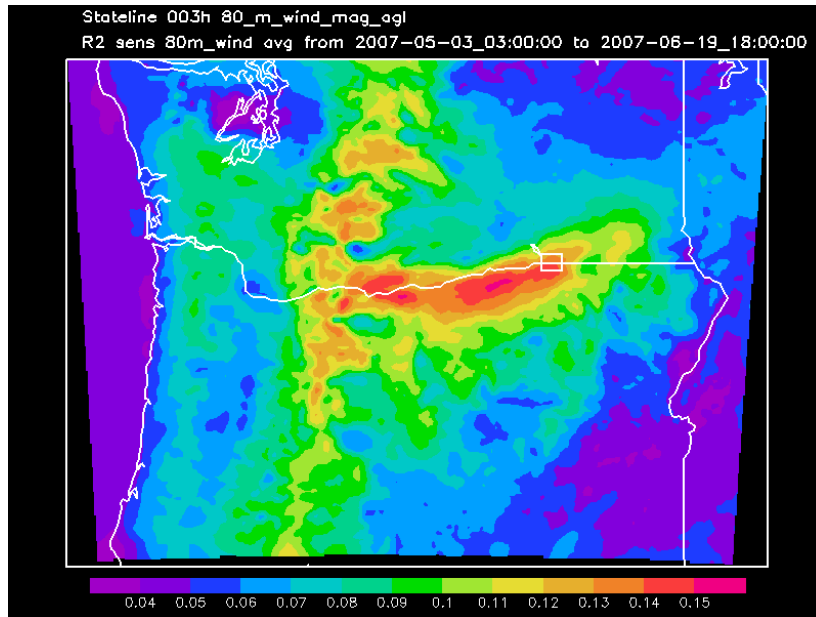


Figure F14. Average R^2 of 80-m wind speed (m/s) within the white target box to the 80-m wind speed throughout the entire grid domain for a 3-hour ahead forecast at all time periods in the 47-day analysis period for Stateline.

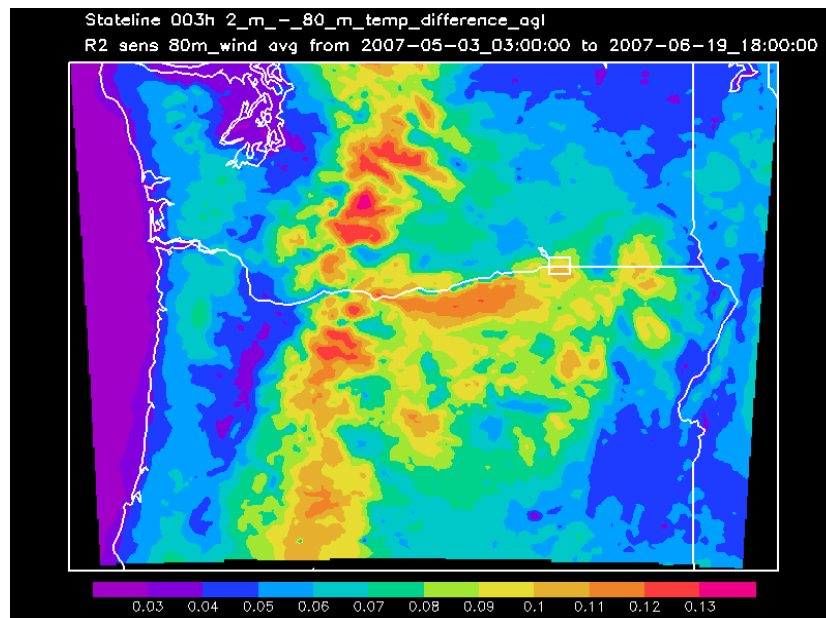


Figure F15. Average R^2 of 80-m wind speed (m/s) within the white target box to 2-m to 80-m temperature difference throughout the entire grid domain for a 3-hour ahead forecast at all times in the analysis period for Stateline.

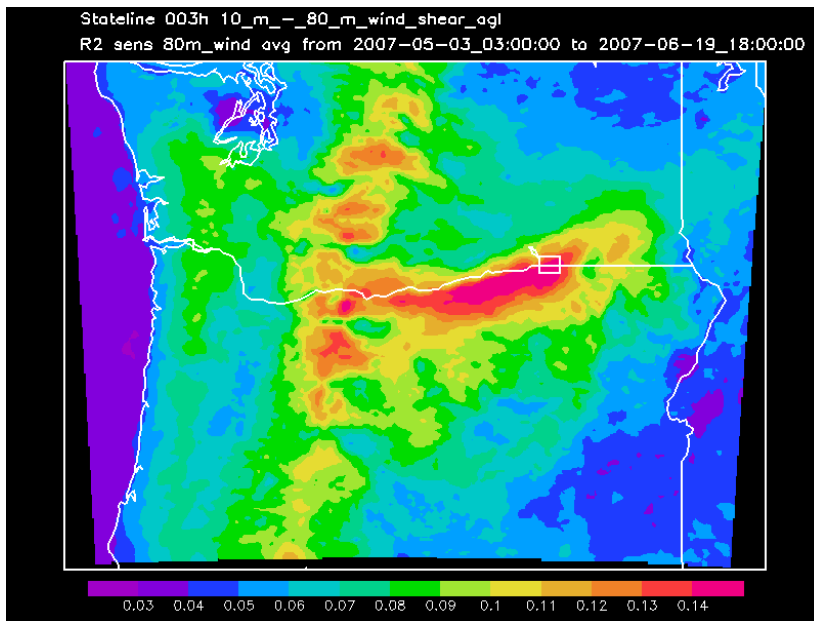


Figure F16. Average R^2 of 80-m wind speed (m/s) within the white target box to 10-m to 80-m wind speed difference throughout the entire grid domain for 3-hour ahead forecast at all times in the analysis period for Stateline.

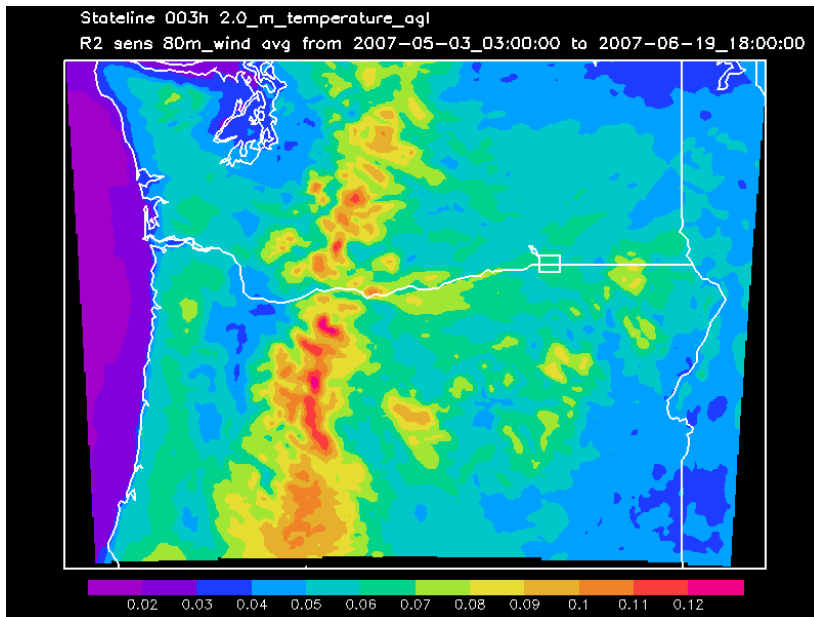


Figure F17. Average R^2 of 80-m wind speed (m/s) within the white target box to 2-m temperature throughout the entire grid domain for a 3-hour ahead forecast at all times in the analysis period for Stateline.

3-Hour Ahead Klondike

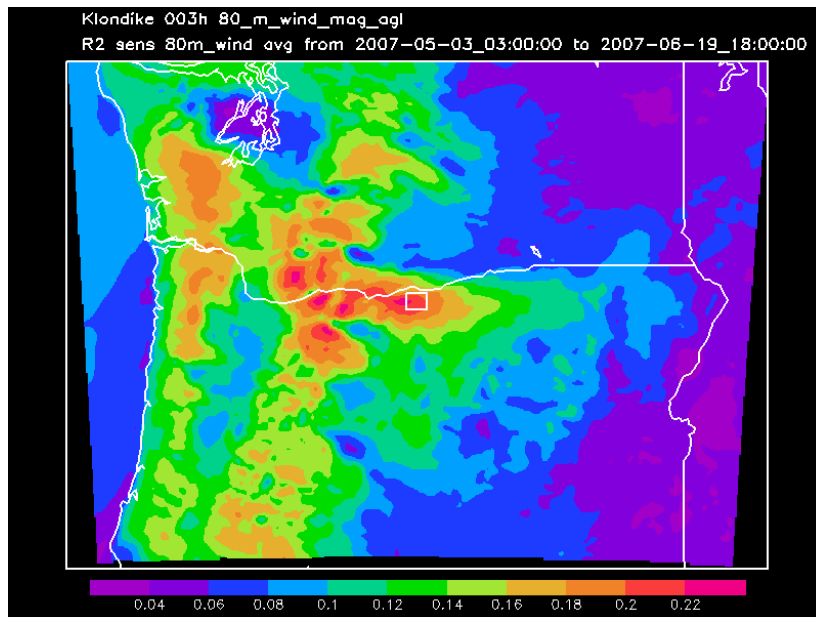


Figure F18. Average R^2 of 80-m wind speed (m/s) within the white target box to the 80-m wind speed throughout the entire grid domain for a 3-hour ahead forecast at all time periods in the 47-day analysis period for Klondike.

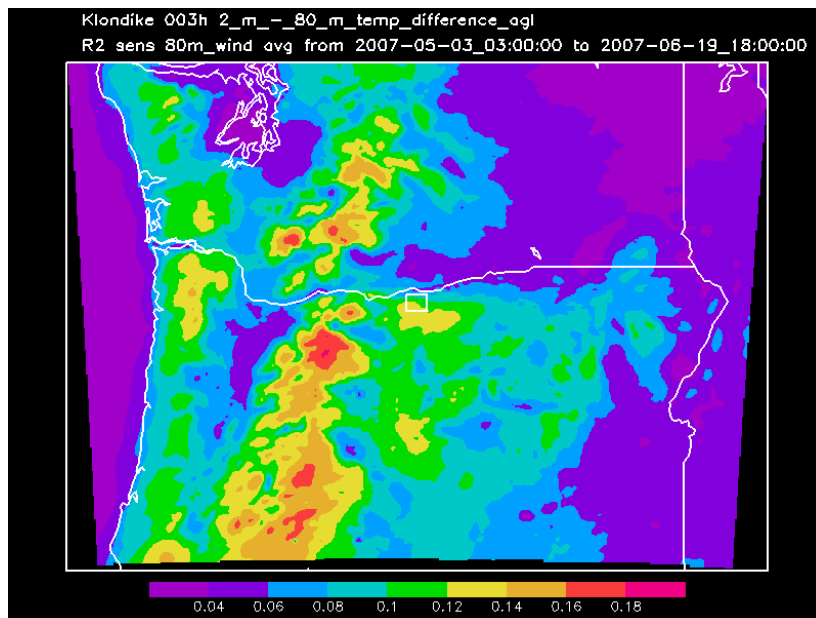


Figure F19. Average R^2 sensitivity of 80-m wind speed (m/s) within the white target box to 2-m to 80-m temperature difference throughout the entire grid domain for a 3-hour ahead forecast at all times in the analysis period for Klondike.

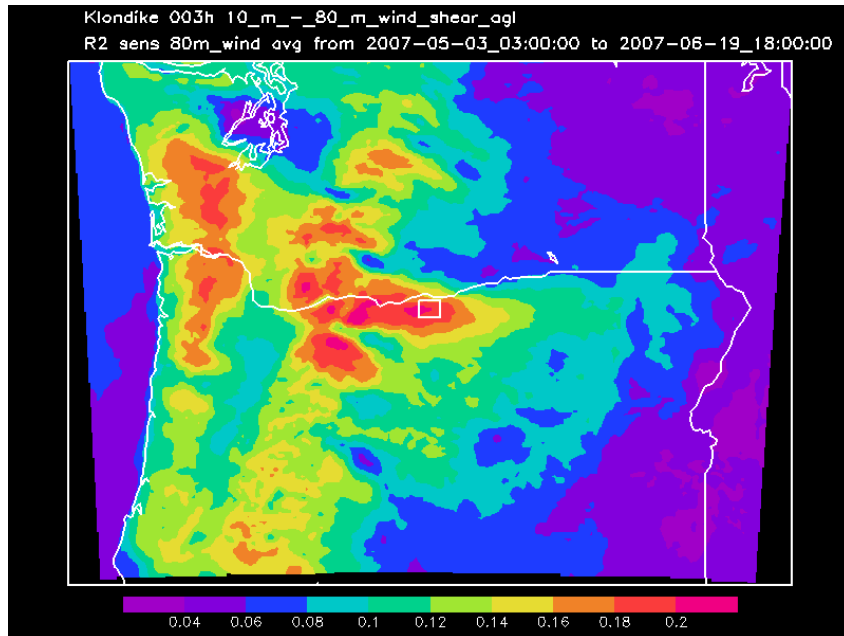


Figure F20. Average R^2 sensitivity of 80-m wind speed (m/s) within the white target box to 10-m to 80-m wind speed difference throughout the entire grid domain for a 3-hour ahead forecast at all times in the analysis period for Klondike.

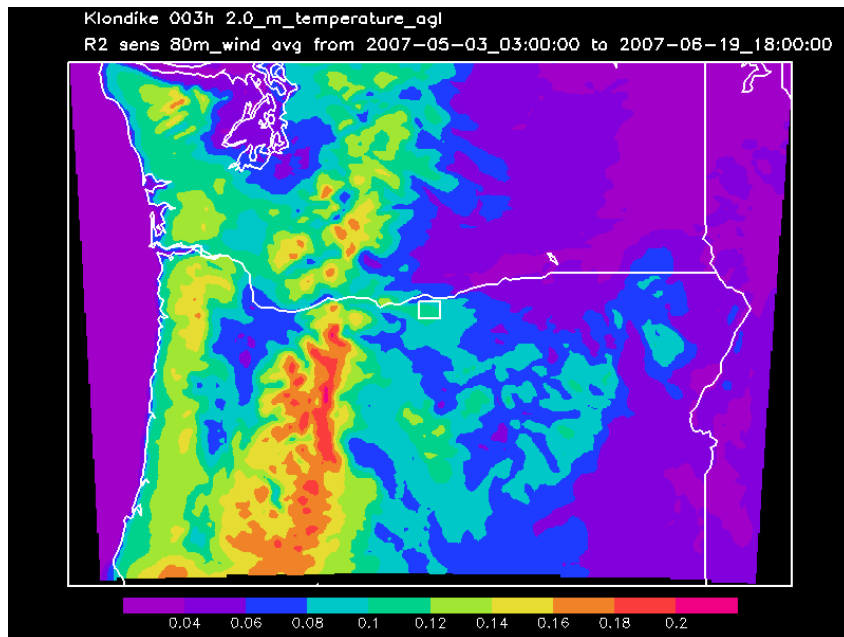


Figure F21. Average R^2 of 80-m wind speed (m/s) within the white target box to 2-m temperature throughout the entire grid domain for a 3-hour ahead forecast at all times in the analysis period for Klondike.

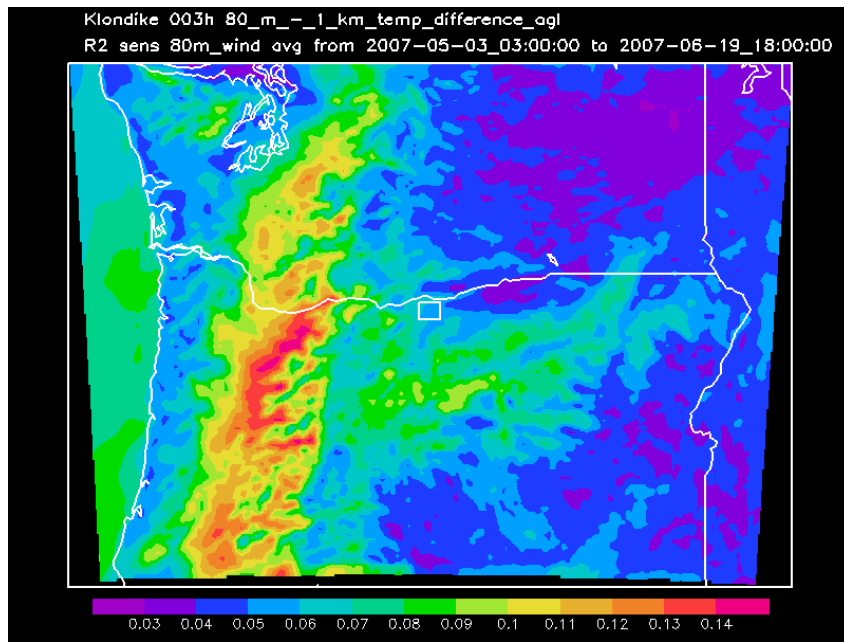


Figure F22. Average R^2 of 80-m wind speed (m/s) within the white target box to 80-m to 1-km temperature gradient throughout the entire grid domain for a 3-hour ahead forecast at all times in the analysis period for Klondike.